Nano-Textured Wick in Heat Pipes

BY

PRATISH SHINDE

B. E., Savitribai Phule Pune University

THESIS

Submitted as partial fulfillment of the requirements

for the degree of Master of Science in Mechanical Engineering

in the Graduate College of the

University of Illinois at Chicago, 2020

Chicago, Illinois

Defense Committee:

Alexander L. Yarin,	Chair and Advisor
Roberto Paoli,	Mechanical and Industrial Engineering
Vitaliy Yurkiv,	Mechanical and Industrial Engineering

This thesis is dedicated to my mother, Dr. Swati Prakash Shinde and my father, Prakash Khandu Shinde, without whose love and support it would never have been accomplished.

ACKNOWLEDGEMENTS

I would like to begin by giving thanks to my Heavenly Father, for it is solely because of Him that I was able to reach until this point in my career.

Words cannot express how grateful I am to my advisor, Distinguished Professor Alexander Yarin. It truly has been an honor and a privilege to have worked with Dr. Yarin since the first day of me joining his lab. I admire him for how knowledgeable he is and how lucidly as a "guru" he explains even the most difficult subjects in engineering and science. Without his constant support and motivation, this work would never have been accomplished. I am grateful to him for all the times he has been patient and uplifted me and given me a push whenever I was stuck on something. I am grateful to him for making math and physics so interesting. I also feel indebted to him for how supportive and generous he has been in funding my research and my tuition through the course of my master's degree.

I am thankful to my thesis committee members Dr. Roberto Paoli and Dr. Vitaliy Yurkiv for their significant support towards making my work worth much more by their valuable comments and queries about the work. I thank them both for their approval and support to jury my work.

I am grateful to my parents for how supportive they have been in uplifting me, countless number of times that I have fallen. It is by the fruits of their labor, that I was able to pursue and initiate my academic life here, at UIC. Their sacrifices have bought for me this gift which I will receive upon graduating from this university. Their love and faith have always been a powerful motivator.

ACKNOWLEDGEMENTS (continued)

I am sincerely thankful to my lab mate, Abhilash Sankaran for his genuine and selfless help in working with me and guiding me from his experience in this research work. I would also like to express a token of gratitude to Dr. Seongpil An who has been of great help since the beginning of my time in this lab. I would also like to thank David Mecha who has been a great supporter and has helped me with the fabrication of the experimental setup and always being ready to help me and fix or modify the setup whenever it was needed.

Many thanks to the famous duo “Chris and Pat”, (Dr. Christopher Staszel and Dr. Patrick Comiskey) for their support and guidance in walking me through the initial stages of my life as a researcher. I am thankful to Dr. Wenshuo Zhang, who has been of great help especially in helping me understand complex concepts. I express gratitude to my lab mates; Kailin Chen, Vinod Balakrishnan, Jingwei Wu, Gen Li, Yasmin Dias and Jevon Plog for their constant support and making lab life so much fun.

I am thankful also to my friends: Maddie Nowak, Tim Bierma, Daniel Sahyouni, Fr. Connor Danstrom and Phillips George for standing next to me when in need and for their authentic friendship.

TABLE OF CONTENTS

TABLE OF CONTENTS (continued)

LIST OF FIGURES

LIST OF FIGURES (continued)

LIST OF FIGURES (continued)

LIST OF ABBREVIATIONS

AAO	Anodic aluminum oxide
CHF	Critical heat flux
CNT	Carbon nanotube
DI water	Deionized water
DMF	N, N-dimethylformamide
GO	Graphene Oxide a.k.a. Reduced graphene oxide
IHP	Integrated heat pipe
K	degree Kelvin
LHP	Loop heat Pipe
PAN	Polyacrylonitrile
PEEK	Polyether ether ketone
PS	Polystyrene
PTFE	Polytetrafluoroethylene
SEM	Scanning electron microscope

SUMMARY

The goal of this work is to investigate the performance of nanofibers in a Loop Heat Pipe. Heat pipes are cooling devices widely used in many domains of the society. The simplicity of their operation combined with their ease in manufacturing makes them suitable for almost every type of cooling application. A lot of research has been done on typical heat pipes which have macroporous wicking materials. However, very less literature is available on use of microporous and nano porous subjects as wicking materials in a Loop Heat Pipe. Nanofibers are thin strands of hair like fibers with the diameter of several hundreds of nanometers. Because of the porous nature of a nanofiber mat, which is nothing but a non-woven subject, the nanofiber pores prove as effective conduits for the passage of working fluid over the heated surface or a surface from where heat is to be taken away. These conduits imbibe and help to pump the working fluid because of capillary effect. Heat absorbed by the working fluid causes it to change its phase form liquid to gas and hence evaporate and later condense elsewhere which is reabsorbed back in the wick. A continuous flow of working fluid is maintained because of the capillary pumping provided by the wick material.

The first part of this work involved an intensive literature review of the already existing and up to date research on enhancing the performance of Loop Heat pipes, particularly by use of micro and nano sized subjects as wicking materials.

Theory was developed to further estimate the important parameters which affect the performance of a heat pipe. This included the mass balance and thermal balance equations, the equation of state of vapor and the volume balance equation in an evaporator chamber. These equations were solved for the steady state operation of the Loop Heat Pipe.

SUMMARY (continued)

A design of an experimental setup of a Loop Heat Pipe was proposed to measure, estimate and cross verify the important performance parameters of a Loop Heat Pipe such as heat flux, substrate surface temperature, mass flow rate of the working fluid. This was followed by computer aided designing and drafting of the proposed heat pipe model. A heat pipe assembly conforming to these designs was fabricated and put together

The experimental setup was tested for the performance parameters which were recorded and further used for estimation and calculation of the parameters. The nanofibers were optically analyzed by use of scanning electron microscopy. A flat electrical heater was used to supply heat as input to the system, the voltage and current for which was measured continuously and was used to calculate the heat flux based on input. An aluminum block served as the heater or "system" from which heat is to be carried away, the temperature for which was measured at known distances and time intervals throughout its cross section. This data was used to calculate temperature gradient through the aluminum block which was then used to calculate the heat flux based as well as the substrate surface temperature. A flowmeter was used to measure the volumetric flowrate of working fluid through the loop at known time intervals. This data was used to calculate the heat flux based on mass flowrate of the working fluid. Three cases with four trials each were performed to evaluate the aforementioned performance parameters of nanofibers as wick materials in the Loop Heat Pipe setup. The three cases were no nanofibers as the primary wick, thin layer of nanofibers as primary wick and a thick layer of nanofibers as primary wick. The individual results were then compared to each other and conclusions drawn to test the case of performance of nanofibers as wick materials in a Loop Heat Pipe.

CHAPTER 1

INTRODUCTION

1.1 Heat pipes

Heat pipes are cooling devices which work on the famous ‘capillary effect’ principle. In simple terms, heat pipes essentially consist of a pours material which is saturated by a working fluid. The saturated wick is enclosed in a leak proof container. The working fluid propagates throughout the wick by the capillary effect principle. When heat energy is supplied to one of the ends, the working fluid evaporates and diffuses towards the other end which is maintained at a lower temperature. After reaching the low temperature zone, the working fluid condenses into liquid form and gets absorbed back into the wick pores and propagates through the wick by virtue of the capillary effect. The porous wick is an important component of the heat pipe. However, heat pipes which do not have a wicking material also exist. Heat pipes are also classified according to their structure, an important one being Loop Heat Pipe (LHP). Loop heat pipes are simple, yet efficient cooling devices used extensively with their applications ranging from cooling of microelectronics to nuclear power cells in spacecraft [Zohuri (2011)]. LHP comprise of an evaporation chamber and a condensation chamber in combination with a condenser connected to it with vapor and liquid lines. LHP also incorporate a wicking structure which is based on capillary suction of the working fluid which is in liquid form to the evaporation chamber. In the latter the latent heat of evaporation removes the energy from the heater, which supplies heat to the chamber bottom. Then, vapor released to the condensation chamber condenses (thus, returning the latent heat elsewhere), and the condensate is resupplied by the wick to the evaporation chamber once again. Nanofiber mats represent a potentially attractive alternative to the commonly used wicking fabrics. Electro spun or solution-blown nanofibers form nonwoven mats with pores in the 2-50 μm range, respectively [Yarin A. L. et. al. (2014)]. The tiny interconnected pores are attractive conduits for capillary suction of working fluid.

1.2 Thesis objectives

The present work aims at improving the performance of heat pipes for ground and space applications. Here, solution blown nanofibers made of polyacrylonitrile (PAN) are used as the wicking material in LHP. An experimental setup was fabricated to do the same and emphasis was given to experimental as well as theoretical understanding of performance of nanofibers in an LHP. Chapter 4 describes the theoretical background of the LHP. Chapter 5 discusses the materials used for fabrication and assembly of the experimental setup. Chapter 6 gives a detailed description of the fabrication and assembly of the setup. Chapter 7 discusses the results and findings of the experimental work and its correlation with the theory. Conclusions are drawn in Chapter 8.

CHAPTER 2

BACKGROUND AND LITERATURE SURVEY

2.1 Wicking in porous subjects

Capillarity and porosity of nanofibers play an important role in the "wicking characteristics" in a heat pipe. The main purpose of a wick is to constantly supply the working fluid to the evaporator from the condenser by virtue of capillary effect. However, at the same point of time it should also allow for the vapor which is formed to leave the wick structure. This constant supply of water should be maintained throughout the time that a heat pipe is in operation [Zohuri B. (2011)]. Failing which, a dry out can occur leading to "runaway condition" post the occurrence of critical heat flux (CHF), a condition in which the heat flux remains constant, but the temperature increases rapidly [Carey V. P. (2007)]. This condition can prove to be severely disastrous to the system itself and the heat pipe causing effects like melting due to high temperature as well as carbonization.

The most frequently used wick materials are metallic and non-metallic felts as well as meshes of varying pore size. Glass fiber meshes are also a common type of wicking material in LHP [Reay D. et. al. (2006)]. However, a majority of those felts and meshes have macroporous pore size. The pore size is a strong deciding factor when it comes to capillarity as well the capacity to hold working fluid. Broad literature is available on the study of macroporous subjects. However, studies have also been done in the past to explore the capillarity and porosity of nano and micro fibrous structures. Lembach et. al. have shown the effectiveness of polyacrylonitrile (PAN) electrosupn nanofiber mats of the pore size of 5μm, the nanofiber diameter being several hundreds of nanometers and porosity 90-95%. Water was observed to have penetrated easily in case of nanofiber mats indicating their high wettability. It was also stated that thicker nanofiber mats have a higher water retaining capacity as compared to their macroscopic and microscopic counterparts pertaining to their high porosity [Lembach A. et. al (2010)]. An et. al have also compared the imbibition speed of a 65 μm thick nanofiber mat against a 135 μm thick nanofiber mat concluding the latter one to be faster in imbibition [An S. et. al. (2017)].

2.2 Nanofibers to enhance cooling

Work has been performed in past to utilize nanofibers to enhance cooling. Heat flux as high as 0.6 kW/cm^2 has been achieved experimentally by use of metal coated nanofibers [Sinha-Ray S. et. al. (2011)]. Sankaran et. al. has demonstrated use of electrically assisted supersonically blown PS nanofibers for pool boiling enhancement with heat flux higher than 100 W/cm^2 in pool boiling phase accompanied by reduction in the surface superheat by 5 K- 6 K when compared to pool boiling over bare substrate surface [Sankaran A. et. al. (2018)]. Freystein et. al. have demonstrated the use of electrospun PAN nanofibers on a mini-channel surface to achieve a heat flux of 3.61 W cm^2 which was 1.6 times higher than bare mini channel surface [Freystein M. et. al. (2014)]. Sahu et. al. have also demonstrated use of PAN nanofibers obtained by a similar technique to enhance pool boiling, heat flux for which was more than 20 W/cm^2 and the surface super heat observed to have reduced by 5 K - 6 K [Sahu R. P. et. al. (2015)]. Fischer et.al. has reported to have obtained a heat flux of magnitude over 1 W/cm^2 upon coating the substrate surface with PAN nanofibers which was 60% more than that without nanofiber coating [(Fischer S. et.al. (2017)]. Sinha and Yarin reported heat flux as high as 0.9 kW/cm^2 by use of copper plated PAN nanofibers on the substrate surface [(Sinha-Ray S. and Yarin A. L. (2014)]. Similar work has also been reported by the same group with emphasis given on enhancing cooling using nanofibers for vivid applications [Sahu R. P. et. al. (2016); Sinha-Ray S. et. al. (2017); Srikar R. et. al. (2009); Sinha-Ray S. et. al. (2017)].

2.3 Micro and nanostructures to enhance pool boiling

Attempts have been made to test the performance of micro and nano surfaces to enhance heat transfer during boiling. Dong. et. al. have shown that use of nano-structured substrate surfaces for pool boiling can lead to enhanced capillary wicking and can further lead to enhanced bubble departure frequency [Dong L. et. al. (2014)]. Weibel and Garimella performed experiments using sintered copper microporous structures coated with carbon nanotubes (CNT) and have reported to have obtained heat flux over 500 W/cm^2 [Weibel J. A. and Garimella S. V. (2012)]. Using methanol as the working fluid, a maximum heat flux of 35.12 W/cm^2 was acquired during pool boiling using copper micro and nanostructures fabricated by laser ablation technique at 85°C by Xueli Wang [Wang X. (2018)]. Attempts have also been made to improve the surface characteristics of the micro-nanostructures to facilitate boiling. Jo et. al. have used graphene oxide (GO) coated copper substrates and it was observed that the GO coating improves boiling heat transfer as it facilitates more nucleation sites [Jo H. et. al. (2018)]. Hu et. al. have reported to have obtained a heat flux of 12.5 W/cm^2 on an aluminum substrate coated with aluminum oxide (AAO) nano porous texture finish coating which was 112% higher than that of the usual aluminum surface. Sintered wicks of various packing densities made of carbonyl nickel powders were fabricated and tested in an LHP and it was found that the pore size and porosity play a critical role in building the capillary pressure [Wang. D. et. al. (2014)]. Performance of an LHP using sintered powder wicks was studied by Ji et. al and it was found that the heat pipes could reach a maximum heat flux of 40 W/cm^2 for the antigravity operation with the wall temperature being 63°C [Ji. X. et. al. (2017)].

2.4 Significance of filling ratio in an LHP

One of the important aspects which affects the operation of an LHP is the filling ratio. It is the ratio of the volume of the working fluid to the total volume of the heat pipe. Almost all the heat pipes have an optimum filling ratio– which is the ratio at which the heat pipe performs the best for a certain input heat flux. Work done by Putra et. al. has shown the importance of liquid to vapor filling ratio on heat pipe performance. The work involved measurement of temperature using neutron radiography and pressure in a heat pipe. It was found that 50% filling ratio was optimum at which the evaporator temperature was the least [Putra et. al. (2015)]. Similar numbers were reported by R. Rabiee et. al. in his work which is about experimental and theoretical analysis of boiling inside a heat pipe [Rabiee R. (2019)]. A filling ratio of 30% was found to be optimum by Thariyal et. al. as mentioned in their work on a flat plate miniature loop heat pipe [Thariyal T. (2016)]. A filling ratio of 30% was also found to be optimum by Ling et. al based on their work on LHP with smooth and rough porous copper fiber wicks [Ling W. et al. (2017)]. Khalili et. al. have investigated the thermal performance of a sintered wick heat pipe and have found that a filling ratio of 20% gives the best performance [Khalili M. et. al. (2016)]. In a study done by Li et. al. it was established that at low filling ratios, the startup characteristic is better whereas at higher filling ratios, the heat pipe can operate at high heat load [Li. H. et. al. (2015)]. A filling ratio of 30% was found to be optimum by Ling et. al. [Ling W. et. al. (2017)]. A filling ratio of 60% was found to be optimum for an integrated heat pipe (IHP) by Wang et. al. [Wang et. al. (2019)].

CHAPTER 3

RESEARCH OUTLINE

Heat pipes are proven to be efficient and effective cooling devices which can be designed and manufactured to easily suit the application depending upon its complexity. Loop heat pipes particularly are of interest because of their flexibility which comes from their ability to have cooling and heating zones at desired distances. Vast literature is available which discusses the performance of macroscopic porous subjects as wicking materials in a heat pipe. Literature is also available on use and performance of micro and nanostructured metallic subjects as wicking materials. However, studies have not been performed on use of nanofibers as wicking materials in a heat pipe. As discussed in the objectives section, this work primarily focuses on use of polymer nanofibers as wicking materials in an LHP. A theory describing important performance parameters such as heat flux, mass flowrate and substrate surface temperature in a typical LHP was developed which was followed by development of a detailed design of an experimental setup to measure and calculate the respective performance parameters experimentally. Required materials to put together the experimental setup were purchased which was followed by fabrication and assembly of the experimental setup. The experimentation was conducted in three phases whereby input power, temperature and working fluid flowrate measurements were measured at known time intervals. Respective heat flux and substrate surface temperature values were calculated based on the acquired experimental data. Electron microscopy was done to analyze the substrate surface characteristics for all the three cases optically. Heat flux and substrate surface temperature plots were produced to visualize and compare the respective similarities and differences in the individual cases. A comparison of theoretical and experimental parameters was also discussed. Conclusion were drawn based on the obtained data.

CHAPTER 4

THEORETICAL

Consider the heat pipe operating at an arbitrary heat flux of $q_i" =$ 100 W/cm^2, which is typically very high in comparison to actual heat flux. The latent heat of evaporation of water which is the working fluid is I = 2 $\times 10^3$ J/g. Let the area of the evaporator, S = 6.25 cm^2. Hence, the theoretical evaporation rate of vapor at the exit of evaporator, $dm_{v,th}/dt$ can be expressed as,

$$\frac{dm_{v,th}}{dt} = \frac{q_i"}{I} S \tag{1}$$

This yields the value 0.3125 g/s for $dm_{v,th}/dt$. The theoretical volumetric flow rate can be calculated by the formula

$$\frac{dV_{v,th}}{dt} = \frac{dm_{v,th}}{dt} \frac{1}{\rho} \tag{2}$$

Where, the density of working fluid, $\rho = 1$ g/cm^3. Hence, $dV_{v,th}/dt$ = 0.3125 g/s. Now consider the evaporator tubing with radius, $a =$0.375 cm and area, $A =$0.442 cm^2. The theoretical flow velocity of vapor, U_{th} in the tube can be calculated by expression

$$U_{th} = \frac{dV_{v,th}}{dt} \frac{1}{A} \tag{3}$$

Hence the vapor velocity in the pipe, $U_{th} =$0.707 cm/s. The Reynold's number, Re for this flow can be calculated using the formula,

$$\mathrm{Re} = \frac{2U_{th}a}{\nu_{vapor}} \tag{4}$$

Where, ν_{vapor} is the kinematic viscosity of vapor and is equal to 0.1 cm^2/s. Thus, Re = 5.303 Similarly, Reynold's number for $q_i" =$ 1 kW/cm^2 can be calculated as 53.03

Hence, it can be said that the vapor flow in the evaporator tube and at the exit of evaporator will always be laminar even if the heat flux is in the range of 1kW/cm^2. This means that Poiseuille flow can be considered for the flow of vapor through the evaporator tube. Also, consider a case when the vapor in the evaporator tube condenses in the tube itself. Thus, using the same set of equations above but replacing ν_{vapor} by $\nu_{water} = 10^{-2}$ cm^2/s we get the following values for Reynold's number:

$$\mathrm{Re}_{water} = 53.025 \text{ for } q_i'' = 100 \text{ W/cm}^2 \text{ and } \mathrm{Re}_{water} = 530.25 \text{ for } q_i'' = 1 \text{ kW/cm}^2$$

Hence, in both the cases i.e., vapor or condensate or even in a case of vapor plus condensate flow through the evaporator tube, Poiseuille flow can be considered.

Consider the evaporation chamber of the heat pipe. The thermal balance for the same can be expressed by the equation,

$$\frac{dm_{l,th} + m_{v,th} c T_{surf,th}}{dt} = -S_{tc} h (T_{surf,th} - T_\infty) + \frac{dm_{l,th}}{dt} I + q_i \tag{5}$$

where, $m_{l,th} =$ mass of liquid in the evaporator chamber is given in gram; $m_{v,th} =$ mass of vapor in the evaporator chamber is given in gram; specific heat capacity of the fluid in the evaporator chamber, $c =$ 4200 J/(g °C)); $T_{surf,th} =$ theoretical substrate surface temperature is taken in degree Celsius; the total surface area of the chamber calculated from geometry, S_{tc} = 11.16 cm^2; heat transfer coefficient of the vapor, $h =$0.5 W/ (cm^2 C); $T_\infty =$evaporator wall surface temperature is taken in degree Celsius; $dm_{l,th}/dt =$ theoretical mass flow rater of water through the loop is given in gram per unit second and $q_i =$ heat supplied via the source is taken in Watt. Here, the expression $[-S_{tc} h (T_{surf,th} - T_\infty)]$ determines the heat lost through the evaporator chamber walls and the expression [$(dm_{l,th}/dt)I$] determines the latent heat of evaporation gained by the working fluid in order to transition from liquid to vapor.

The mass balance can be given by the equation,

$$\frac{d(m_{l,th}+m_{v,th})}{dt} = S_{wick}\frac{\sigma 2a_p\cos\theta}{8v_e L_{wick}} - \frac{\pi a^4}{8v_e}\frac{[p_{sat}(T_{surf,th}) - p_{atm}]}{L_e} \tag{6}$$

where, cross sectional area of the secondary wick exposed to the evaporator chamber by geometry, S_{wick} = 0.78 cm^2; surface tension of water, $\sigma = 72$ dynes/cm; pore radius, a_p = 10^{-4} cm; contact angle, $\theta = 0$; kinematic viscosity of water, $v_e = 10^{-2}$ cm^2/s; length of the secondary wick from compensation chamber to the evaporation chamber by geometry, $L_{wick} = 1.5$ cm; $p_{sat}(T_{surf,th}) =$ saturated vapor pressure is given in dyne/cm^2 (1 dyne/cm^2 = 10^{-3} mbar); atmospheric pressure, p_{atm} = 1013250 dyne/cm^2 = 1013.25 mbar and length of the evaporator tubing, L_e = 12 cm

The equation of state of vapor can be expressed as,

$$p_{sat}(T_{surf,th})V_{vapor,th} = \frac{m_{v,th}}{M_w}RT_{surf,th}$$

(7)

Where $V_{vapor,th}$ =theoretical volume of vapor in the evaporator chamber is taken in m^3; molecular weight of water vapor, $M_w = 18.02$ g/mol and ideal gas constant $R = 8.3145$ J/(mol K)

The volume balance can be given by the equation,

$$V_{vapor,th} = V_{chamber} - \frac{m_{l,th}}{\rho_l} \tag{8}$$

where, volume of the evaporator chamber, $V_{chamber} = 2.34$ cm^3 and density of the working fluid, ρ_l = 1 g/cm^3

Consider the heat pipe to be in a steady state. Hence, $d(m_{l,th}+m_{v,th})/dt=0$ and $dT_{surf,th}/dt=0$

From equation (6) we obtain,

$$\left[p_{sat}(T)-p_{atm}\right]=\frac{2S_{wick}\sigma a_p\cos\theta L_e}{L_{wick}\pi a^4} \tag{9}$$

Here $p_{sat}(T_{surf,th})$ and p_{atm} are given in dyne/cm^2 which are then converted to mbar. The saturated vapor pressure can also be calculated using Clausius-Clapeyron, or Antoine equation,

$$p_{sat}(T_{surf,th})=b_0+T_{surf,th}[b_1+T_{surf,th}(b_2+T_{surf,th}\{b_3+T_{surf,th}[b_4+T_{surf,th}(b_5+b_6T_{surf,th})]\})] \tag{10}$$

where $p_{sat}(T_{surf,th})$ is given in mbar, and $T_{surf,th}$ is taken in degree Celsius. The values of the parameters *bi* are stated as follows: $b_0 = 6.107799961$, $b_1 = 4.436518521 \times 10^{-1}$, $b_2 = 1.428945805 \times 10^{-2}$, $b_3=2.650648731 \times 10^{-4}$, $b_4 = 3.031240396 \times 10^{-6}$, $b_5 = 2.034080948 \times 10^{-8}$, $b_6 = 6.126820929 \times 10^{-11}$

This equation can also be written as,

$$p_{sat}(T_{surf,th})-p_{atm}=b_0+T_{surf,th}[b_1+T_{surf,th}(b_2+T_{surf,th}\{b_3+T_{surf,th}[b_4+T_{surf,th}(b_5+b_6T_{surf,th})]\})]-p_{atm} \tag{11}$$

The value of *T* corresponding to $p_{sat}(T_{surf,th})$ is illustrated in Fig. 4.1 whereby the LHS of equation (9) and the LHS of equation (11) is plotted along the vertical axis whereas the temperature, $T_{surf,th}$ in degree Celsius is plotted on the horizontal axis. The intersection of the line for equation (9) and equation (11) projects the value of $T_{surf,th}$ corresponding to $p_{sat}(T_{surf,th})$ which is approximately 99.643 °C

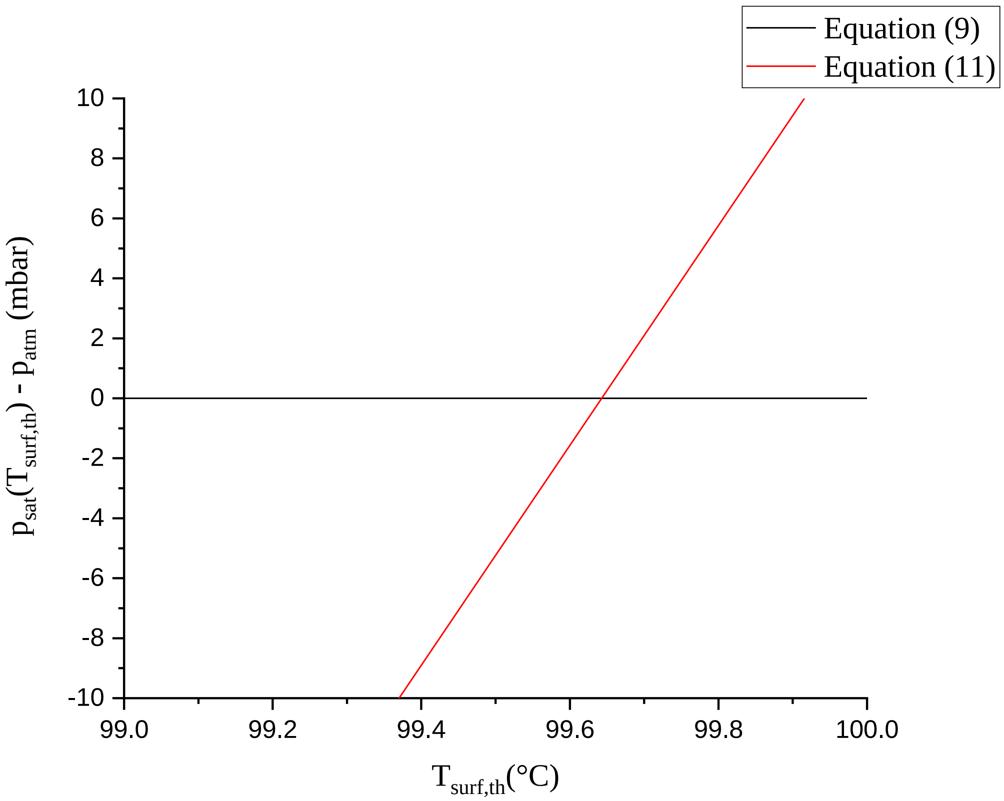

Figure 4.1 The left-hand side of both, equation (9) and equation (11) are shown by black and red lines respectively. Their intersection projects the value of corresponding $T_{surf,th}$ for which is the value of the temperature inside the evaporator chamber.

Also, from equation (5) we obtain,

$$\frac{dm_{l,th}}{dt} = \frac{S_{tc}h(T_{surf,th} - T_{\infty})}{I} - \frac{q_i}{I} \tag{12}$$

This equation can also be written as,

$$-\frac{dm_{v,th}}{dt} = \frac{dm_{l,th}}{dt} = \frac{S_{tc}h(T_{surf,th} - T_{\infty})}{I} - \frac{q_i}{I} \tag{13}$$

which is the equation defining the mass flow rate of vapor exiting the evaporator.

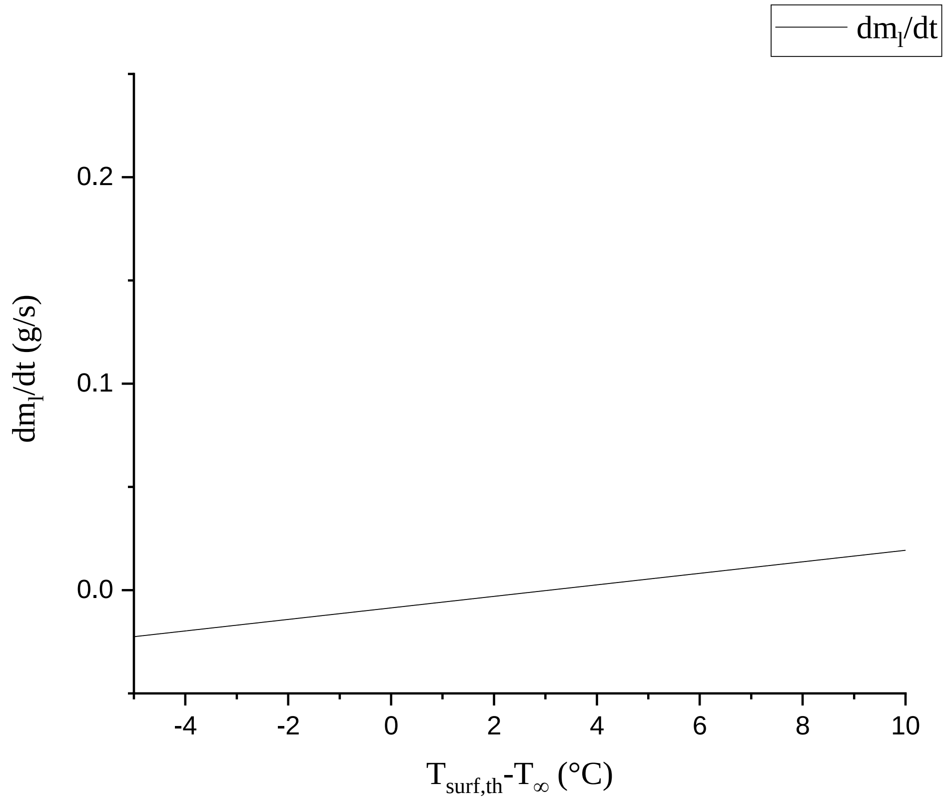

Figure 4.2 A plot of the left-hand side of equation (11) which is $dm_{l,th}/dt$ versus $(T_{surf,th} - T_{\infty})$ indicating the change in the mass flow rate of water in the evaporator chamber with respect to changing evaporator wall temperature at $q_i = 17.5$ W.

The input heat supplied, q_i for all the experimental trials was constant and same throughout the course of experiment which was equal to 17.5 W. Ref. Fig. 4.2 the value $dm_{l,th}/dt$ can be illustrated for varying $(T_{surf,th} - T_{\infty})$ on the plot which very well indicates that for a condition of negligible heat loss to the evaporator chamber wall, the value of $dm_{l,th}/dt$ is negative indicating that the mass of liquid reduces with a consequent increase in the mass of vapor. For a case of no losses when $T_{surf,th} = T_{\infty}$, the mass flow rate of water, $dm_{l,th}/dt$ = 8.59 $\times 10^3$ g/s = 0.515 g/min

CHAPTER 5

MATERIALS AND EXPERIMENTAL SETUP

5.1 Materials

An aluminum bar of dimensions 2.5 cm $\times$ 2.5 cm $\times$ 15 cm and 99.9% purity was purchased from McMaster Carr. The heater, ULTRAMIC, was purchased from Watlow. Thermal paste was purchased from Insignia. Thermocouples and the data logger for the same were purchased from Omega Engineering. Polyacrylonitrile (PAN; M_w= 150 kDa) was obtained from Sigma Aldrich. N-Dimethyl formamide (DMF) was obtained from Fisher Scientific. Cellulose sponge was purchased from Mc Master Carr. Polyether-ether ketone (PEEK), O-ring, teflon insulation, silicone putty, hose clamps and gasket materials were purchased from McMaster Carr. Brass tee connecters, elbow connectors, copper mesh, screws, stainless steel ball valve, three-way valve, Luer locks barbed brass connectors, plastic tubing for condensing fluid and compression fittings were purchased from McMaster Carr. Bendable copper tube to be used as evaporator tube with inner diameter 0.368 cm and outer diameter 0.650 cm was purchased from McMaster Carr. Flexible plastic tubing of inner diameter 0.368 cm and outer diameter 0.650 cm to be used as connection between heat pipe, flowmeter and condenser was purchased form McMaster Carr. SLS-1500 Flowmeter was purchased form Sensirion. 16-gauge stainless steel syringe needle, 15 cm long was purchased form McMaster Carr. 30 ml and 60 ml syringes were purchased from Air-tite. Gorilla glue, 800 grit sandpaper and raw materials for condenser was purchased from McMaster Carr. DC power supply (0V-60V, HY6003D) was purchased from Mastech. AC power transformer 0 V – 130 V was purchased form Tenma. Multimeters purchased from Fluke, 117 Ture RMS and 115 True RMS were used as ammeter and voltmeter respectively.

5.2 Preparation of components

PAN nanofibers were manufactured using solution blowing technique. To do this a solution of 12% v/v PAN was dissolved in DMF at room temperature. The solution was stirred for at least 12 hours. Solution blowing was then done inside a hood. A syringe pump was used to pump the solution at 1.7 ml/hr rate. A 21-gauge needle was used, and air was supersonically blown around the needle to achieve nanofibers of several hundreds of diameters. The nanofibers were collected at the bottom of the setup. This technique is very much similar to solution blowing process described elsewhere [Sinha-Ray S. et. al. (2013)].

Two cuboidal cellulose sponge pieces were first saturated with water and were then fabricated to dimensions 5 cm $\times$ 1.5 cm $\times$ 2 cm each. One of these pieces was coated with solution blown nanofibers in such a way that all the faces of this cuboid were covered by nanofibers. These two sponge pieces were then squeezed together and were made to fit the cavity inside the cover plate such that the resulting fit after insertion of the sponge pair would be a snug fit. This pair of sponges served as the secondary wick itself.

High temperature silicone rubber gasket of 2 mm thickness was first cut to the dimensions corresponding to the geometry at the bottom face of the cover plate. Holes were then punched along its periphery corresponding to that on the cover and base plate.

CHAPTER 6

EXPERIMENTAL

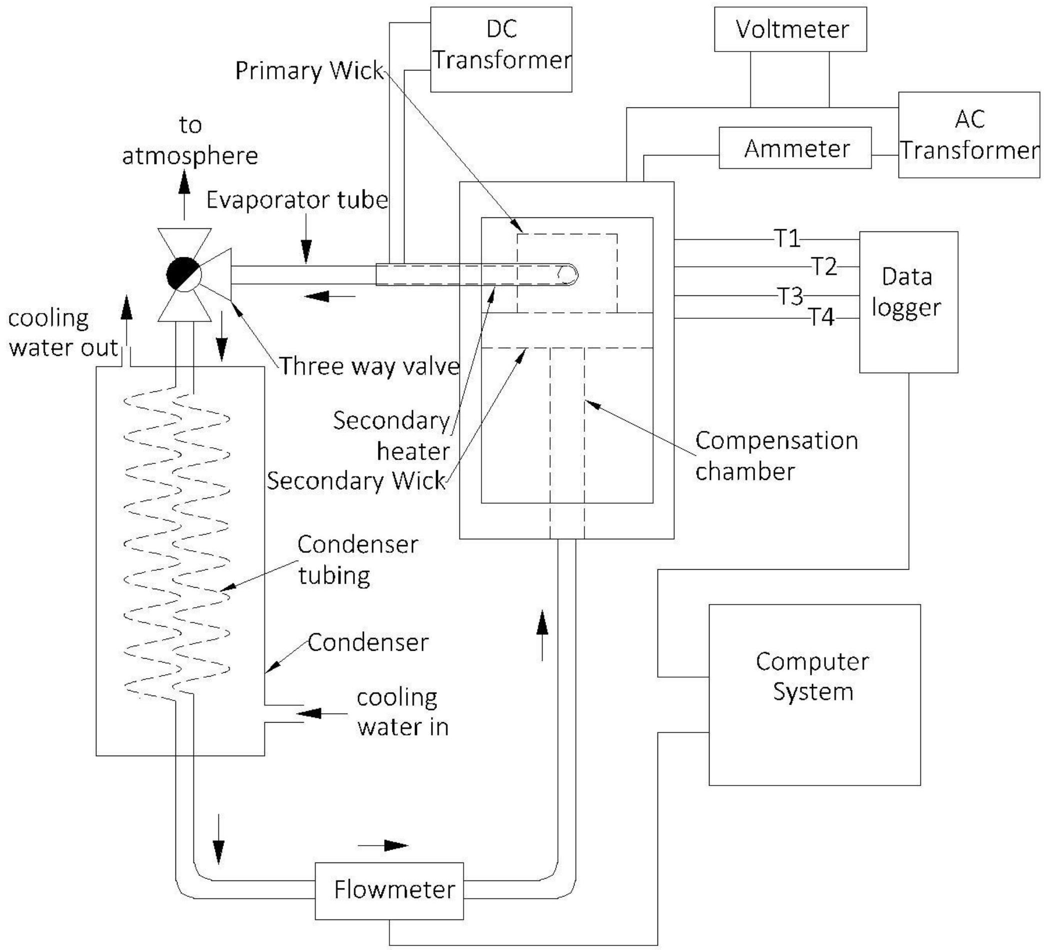

Figure 6.1 A schematic of the experimental setup. This would be a view looking at the setup from the top. The heat pipe assembly is shown in the center which is connected to the condenser via evaporator and condenser tubing. Flowmeter to measure flow as well as valve to control the direction of flow is also shown. The power supply and data acquisition system are also shown.

Ref. Fig 6.1 The experimental setup consists of a heater block embedded at the bottom of the evaporation chamber. A tube in shell type of condenser is used in the heat-pipe assembly in order to enhance condensation of working fluid. Deionized water (DI) was used as the working fluid.

6.1 Prototype fabrication and setup

6.1.1 Heat pipe assembly

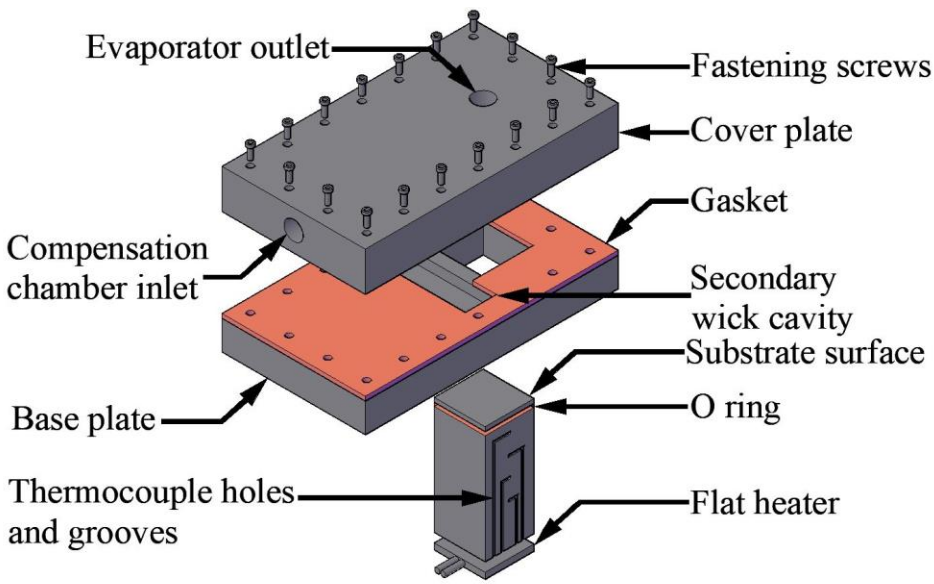

Figure 6.2 Exploded view of the heat pipe assembly. The aluminum heater block connected to the heater is pressed to fit inside of the cavity in the base plate until the substrate surface is coplanar to the top face of the base plate. In cases when necessary, nanofibers are deposited on the substrate surface which is followed by covering them with copper mesh. The cover plate is then fastened to the base plate. Gasket and O-ring are used to attain a leak proof fit.

Ref. Fig. 6.2, The evaporator is a section where boiling takes place. It mainly comprises of a heater base which is the upper surface of the aluminum block henceforth referred to as the substrate surface. The evaporator section can be thought of as a hollow cuboid with one of the walls made up of the substrate surface. This surface represents the area from which heat is to be carried away.

A cuboidal aluminum solid block of dimensions 2.5 cm$\times$2.5 cm$\times$10 cm was fabricated with all the 10 cm long edges chamfered to an arc of radius 0.1 cm. One of the 2.5 cm$\times$2.5 cm surfaces of the aluminum block, which is facing up served as the substrate surface whereas the other 2.5 cm $\times$2.5 cm surface facing down served as the receiving face for heat input via a flat electrical heater. A groove 0.2 cm deep was machined on all the 2.5 cm$\times$10 cm sides of the aluminum block at 0.2 cm from the substrate surface. This was done to allow for a silicone rubber O-ring to fit inside the groove. Four finished holes of diameter 0.05 cm and length 1.25 cm were drilled perpendicular to one of the 10 cm$\times$2.5 cm sides at distances 0.7 cm, 2 cm, 3.5 cm and 5.21 cm respectively from the substrate surface to allow for passage of four T type thermocouples. Four respective grooves for these thermocouples were also milled on the same 2.5 cm$\times$10 cm face in order to accommodate for the thermocouple wires and allow for them to lie coplanar to one of the 2.5 cm$\times$10 cm sides perpendicular to the thermocouple hole. Before insertion the tips of the thermocouples were coated with Insignia thermal paste to allow for a continuous contact with the aluminum block. After insertion, the thermocouples were made to fit inside the grooves of the aluminum block. This aluminum block was then inserted inside an insulation made from PEEK which was machined to conform to dimensions 7.5 cm$\times$13 cm$\times$2 cm henceforth referred to as the base plate. A cuboidal hole of dimensions 2.5 cm$\times$2.5 cm$\times$2 cm was milled through the base plate from top all the way through to allow for insertion of the aluminum block. The aluminum block was inserted 2 cm deep inside the base plate from the bottom side of the base plate upwards such that the substrate surface is coplanar to that of the top face of the base plate. Following this, an electrical heater, henceforth referred to as the primary heater was made to adhere the rear face of the aluminum block by use of the thermal paste which also allowed for a continuous contact of heater surface and the bottom of aluminum block. Thermal insulation, 1 cm thick fabricated using polytetrafluoroethylene

(PTFE) also known as Teflon as the raw material was used to cover the four sides of the aluminum block which was sticking out of the base plate on its bottom side. Insulation was also used to insulate the bottom side of primary heater. Grooves of adequate dimensions in the insulation allowed for a smooth passage of the thermocouple wires as well as the heater wires. The exits of these grooves from which the wired connections were let out were sealed with silicone putty to ensure reinforcing and support to the wiring at these ports and ensure a leak proof fit to avoid seepage of working fluid inside the grooves in an event of mishap. The PTFE insulation around the aluminum block was held together using hose clamps to allow for continuous and a leak proof contact.

The base plate had an additional cuboidal cavity of dimensions 5 cm $\times$ 1.5 cm $\times$ 5 cm milled on its top face to allow for a snug fit of the secondary wick. A rectangular array of 18 threaded holes, 1.5 cm deep which conform to the M 3.5 $\times$ 0.6 standard of threaded holes was also machined along the periphery of the top face of the base plate to allow for a leak-proof fit with that of the cover plate aided by a high temperature silicone rubber gasket conforming to the same dimensions.

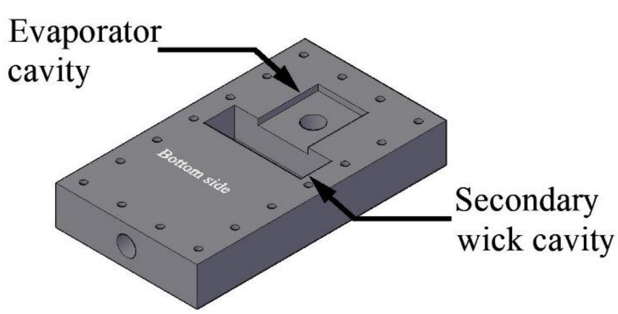

Figure 6.3 Bottom side of the cover plate. Cavities are milled on the bottom side of the cover plate to accommodate the secondary wick as well as to serve as the evaporator chamber. Conduits are machined to serve as the compensation chamber itself as well as the outlet for evaporator tubing.

Ref. Fig 6.3, a cover plate made of PEEK with dimensions 7.5 cm $\times$ 13 cm $\times$ 2 cm was fabricated to serve as an enclosure for the evaporator chamber, an enclosure for secondary wick and as the compensation chamber itself. A cuboidal cavity of dimensions 2.6 cm $\times$ 3.1 cm $\times$ 0.3 cm was milled on the bottom face of the cover plate which corresponds with the dimensions of the substrate surface with a clearance of 0.05 cm on the left, 0.05 cm on the right-hand and 0.05 cm on the front side to avoid it's contact with the substrate surface. This cavity was continuous at rear 2.6 cm $\times$ 3 cm cross section to allow for a continuous channeling with the cavity for secondary wick.

A hole, open at both the ends was drilled through the top face of the cover plate centrally with respect to the evaporator chamber cavity 2 cm from the front 7.5 cm edge. This outlet is a hole of diameter 1.03 cm (corresponds to a standard NPT hole size with 10.3 mm outer diameter for thread) which happens to be threaded to allow for a leak proof fitting of a brass tee connector. This was done to allow for connection with the outlet line which connects the evaporator chamber to the inlet of the condenser so that the vapor formed in the evaporator can travel towards the condenser. A cavity with dimensions 0.5 cm $\times$ 1.5 cm $\times$ 1.5 cm was milled on the bottom face of the cover plate to accommodate the secondary wick. Both respective cavities on the cover plate correspond to the dimensions of the cavity to accommodate the heater block and the cavity for the secondary wick in the base plate. In addition to the respective cavities for the evaporator chamber and the secondary wick, a cylindrical hole, open at both ends of diameter 1.03 cm was drilled from the rear edge of the cover plate all the way through the rear face of the secondary wick cavity to allow for a formation of a continuous channel. This channel served as the compensation chamber. The rear end of this hole corresponding to the rear face of the cover plate was threaded to obtain standard internal NPT threads with a standard major diameter 1.0242 cm. This was done to allow for connection with the outlet of the condenser with the help of an elbow connector. 18 holes with dimensions corresponding to the ones in the base plate were also drilled through the cover plate in order to allow for the cover plate to be fastened with the base plate.

One of the walls of the cuboid mentioned in the first passage of the experimental section is the secondary wick which acts as a porous interface between the evaporator chamber and the compensation chamber. The substrate wall is oriented horizontally and lies within an imaginary plane passing parallel to the horizon whereas the wicking wall is perpendicular to the substrate wall at an angle of 90° to the horizon. This cuboidal structure, henceforth referred to as the evaporator chamber also has an outlet for the vapor to pass upwards by virtue of its low density. Solution blown nanofibers were laid on the substrate surface before the assembly of the base plate and the cover plate. A copper mesh was placed on the top of the nanofibers in order to avoid delamination of the nanofibers from the substrate surface during boiling. This copper mesh was fabricated to dimensions 7.3 cm $\times$ 2.5 cm and it had four holes near its corners for it to fit corresponding to 4 of the 18 screws used to fasten the cover plate to the base plate.

The cover plate was aligned with the base plate to match with the corresponding cavities and holes. The cover plate was then fastened to the base plate with the help of screws in such a way that the remainder of secondary wick which sticks out of the cavity in the cover plate snuggly fits inside the secondary wick cavity of the base plate. A leak proof fit between the cover plate and the base plate was achieved by using a silicone rubber gasket.

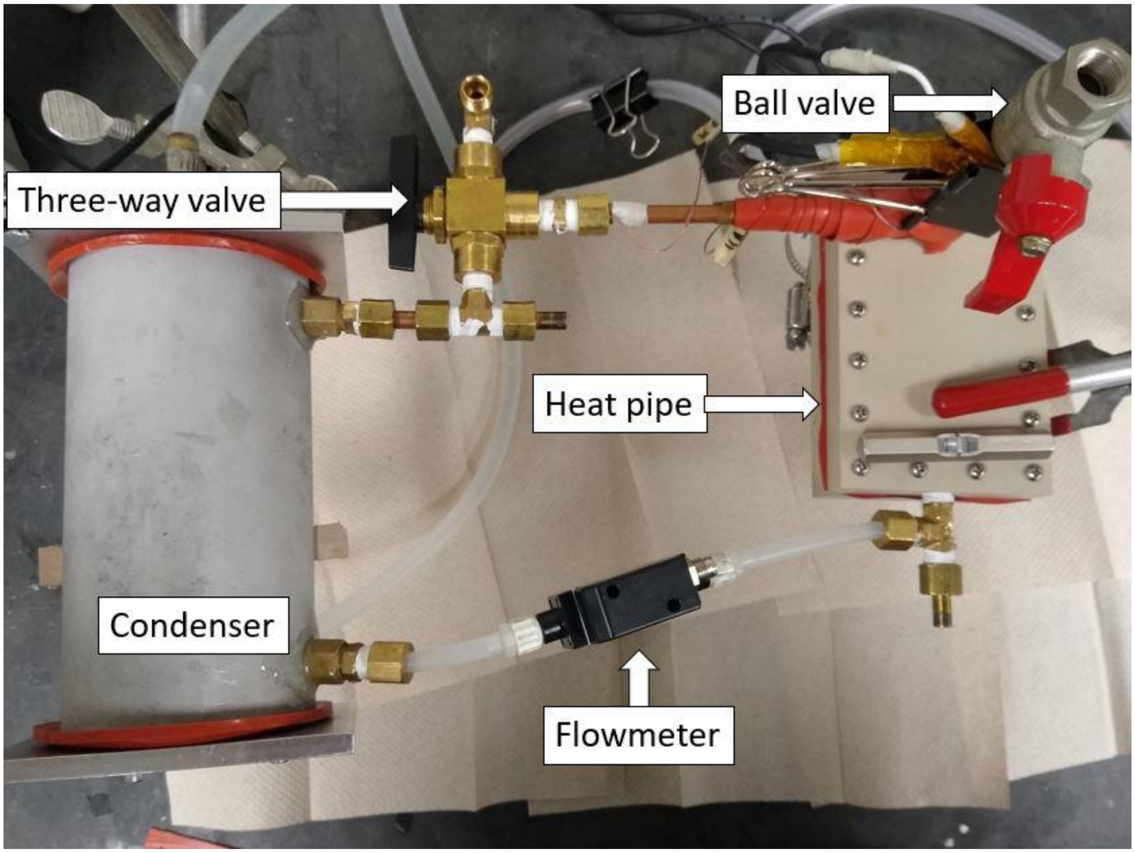

Figure 6.4: An actual photograph of the experimental setup as viewed looking from top. Ball valve is present on the top of the evaporator chamber to allow for charging of the heat pipe. Teflon tape was used to achieve a leak proof fit in combination with compression fittings at all connections All the parts of the experimental setup are shown except the power system and the data acquisition system.

6.1.2 Tubing

Ref. Fig. 6.4, tubing was used to connect the heat pipe to the condenser. There are two parts of the tubing system that is the one which connects the evaporator to the inlet of the condenser and the one which connects the compensation chamber to the outlet of the condenser. A tee connector was used to connect the outlet of the evaporator to the inlet of condenser via a copper tubing, 10 cm long, henceforth referred to as the evaporator tube. Brass compression fittings were used to achieve a leak proof fit. The other end of the tee connector was connected to a stainless-steel ball valve using a similar copper tubing and compression fittings. The ball valve is aligned vertically such that the axis of this valve is collinear to that of the vertical axis of the aluminum block. This valve is used for charging the working fluid in the evaporator chamber before heat pipe startup. The evaporator tube is perpendicular to the axis of ball valve. The evaporator tube further connects with the inlet of condenser with the help of a three-way valve. The inlet of this valve is connected to the evaporator tube and one of its outlets is connected to the inlet of the condenser with the help of a 2 cm long copper tube and compression fittings. The other outlet of the three-way valve is open to the atmosphere. The secondary heater was wrapped around the tee fitting and the evaporator tube such that it covers the evaporator tube up to a length of approximately 5 cm and the ball valve inlet up to a length of approximately 3 cm. This additional heater was used to avoid vapor condensation right at the outlet of the evaporator chamber to further eliminate the dripping of condensate back on the substrate surface. This heater was wrapped around with silicone rubber gasket material to avoid potential heat loss to the atmosphere. Four T type thermocouples were used to measure temperature at four different points outside the evaporator namely, the exit of the evaporator, temperature at 3 cm, 6 cm and 10 cm from the exit of the evaporator respectively. An elbow connector was used to connect the compensation chamber to the outlet of the condenser by use of a plastic tubing. A flowmeter was placed in series with the plastic tubing to measure the flowrate and direction of the flow through the loop. The length of this tubing was 3 cm from the connecter to the flowmeter outlet. A similar tubing of about the same length was used to connect the inlet of flowmeter using Luer lock pair and the outlet of the condenser using brass compression fittings.

6.1.3 Condenser

A shell in tube type of condenser was fabricated to allow for the working fluid to cool down. A hollow cylindrical shell body 15 cm long was fabricated out of aluminum with 7 cm inner diameter and 7.6 cm outer diameter. Copper tubing of considerable length was first coiled around in the shape of a helix of 2.5 cm mean coil diameter with 12 turns and pitch of approximately 0.5 cm. Both the ends of this helical tube were kept straight to a length of 5 cm. Two circular holes of diameter 0.66 cm were drilled about 10 cm apart on the curved surface of the cylindrical shell. Both the ends of the helical copper tube were inserted through these holes and the interface with cylindrical shell was sealed with Gorilla Glue to avoid leakage of condensing fluid. The ends of copper tube served as respective inlet and outlet for the working fluid. Two respective connectors were used at the inlet and outlet to facilitate connection with the evaporator tube and the tubing connecting to the flowmeter inlet.

A circular array of 5 threaded holes each 72° apart was machined on both the circular faces of the cylindrical shell. Two rectangular aluminum plates of dimensions 10 cm $\times$ 0.5 cm $\times$ 7 cm were used to seal both the open sides of the cylindrical shell and two identical silicon rubber gaskets conforming to the dimensions of threaded holes and their geometrical arrangement were used between the interface to achieve a leak proof fit.

An internally threaded circular hole open at both the ends conforming to 17 mm NPT standard of internal threaded holes diameter was drilled radially all the way through the curved surface area of the shell at a distance 2 cm from rear circular face to allow for a leak proof fit with a barbed brass connector. This opening served as the inlet for condensing fluid. A similar hole with an identical connector was fabricated on the front aluminum plate at a suitable location 1 cm below the top face of the plate. The inlet and outlet were connected to the respective supply and drain of water at 25°C by use of plastic tubes. The inlet and outlet plastic tubes were connected to the barbed ends of the brass connectors and two respective hose clamps were used to make sure that the fitting is void of any leaks. The condenser was fabricated in such a way that the resulting assembly would allow for water to fill up the condenser body from bottom towards up and the air to exit the outlet by virtue of its low-density during startup. This setting also helped in maintaining a steady and uniform current of cooling water around the copper tube also referred to as the condenser tubing.

6.1.4 Power system

A 110 V transformer was used to supply electrical power to the primary heater. The voltmeter the in parallel to the outlet of this transformer was used to measure the voltage across the primary heater circuit. An ammeter connected in series with the primary heater circuit was used to measure the current flowing through the circuit. A DC power supply was used to supply electrical power to the secondary heater. It had an inbuilt voltage and current indicator which was used to note down the values of the voltage and current at different points of time through the course of experiment.

6.1.5 Data acquisition system

A data logger was used to measure the temperature across the 8 thermocouples mentioned earlier in the complete system. A computer system was used to acquire data from the data logger over the course of the whole experiment. The same computer system was also used to acquire data from the flowmeter over the course of entire experiment. Current and voltage readings for both the primary heater and the secondary heater were noted down over the course of the experiment.

6.2 Charging and start-up procedure

DI water at 25° C and atmospheric pressure is used as the working fluid in heat pipe loop. The ball valve which is right above the evaporator section is kept in open position. The three-way valve connecting the evaporator tube to the condenser inlet is kept in such a position that the connection from the condenser inlet to the evaporator line is continuous all the way until the inside of evaporator and also to the atmosphere through the ball valve. Initially the flowmeter is disassembled and removed from the loop by disconnecting its Luer Lock connections with the plastic tubing at its inlet and outlet. A 30 ml syringe is used to pump fluid inside the condenser line which constitutes to the part of heat pipe loop. This is done until all the air in the condenser line and the evaporator line is seen to have purged out all the way through the ball valve. The three-way valve is then positioned in such a way that all its ports remain closed. The syringe is then disconnected from the line.

A 16- gauge needle is used in combination with a syringe to pump water inside the evaporation chamber. The needle is inserted inside the evaporation chamber via the ball valve outlet. It is inserted until there is a negligible gap between the copper mesh and the tip of the needle. Water is then pumped inside of the evaporator from the substrate surface upwards until all the air is seen to have purged out of the evaporator. It is then ensured that the primary and the secondary wick are completely saturated, and all the air is purged out of their pores because of the presence of water column until the outlet of the ball valve. The falling level of this water column is constantly replenished until all the air in the compensation chamber is purged out via the plastic tube which is supposed to connect the compensation chamber to the condenser via the flowmeter. During the same time the whole assembly is tilted in such a way that the front end of the heat pipe is slightly below (about -15°), and the rear end of the heat pipe is above an imaginary plane parallel to the horizon. The assembly is held in this position and the water column mentioned earlier replenished until all the air is seen to have purged out of the elbow via the compensation chamber. Similar methodology is used again but the front end now being up and the rear end now being below to purge out the remainder air in the elbow connector at the rear end of the compensation chamber. The flowmeter is now connected to the compensation chamber by connecting it with the plastic tubing. Care is taken to maintain and replenish the water column mentioned earlier until all the air is also seen to have purged out of the flowmeter. The flowmeter is then connected to the condenser outlet. This procedure ensures complete charging of the heat pipe loop.

The ball valve is now closed. The three-way valve connecting the evaporator line to the inlet of the condenser is then positioned in such a way that the connection from the evaporator is continuous to the atmosphere only through the valve outlet. To begin the experiment, the liquid in the evaporator chamber and the evaporator line is boiled vigorously to allow for the all the non-condensable gases to escape the chamber and the evaporator line via the valve outlet. After this the three-way valve is positioned such that the connection from the evaporator is continuous all the way through the evaporator line followed by the condenser line which is followed by the flowmeter and then the compensation chamber. This ensures a closed loop working condition of the heat pipe. All the water evaporated in the evaporator is replenished by the incoming water supply via the secondary and then via the primary wick from the compensation chamber. A steady state is defined as being achieved when the variation of the surface temperature over a span of 60 minutes is less than 0.5° C. The experiment is repeated 5 times and all the data is recorded in the computer system for the temperature and flowrate each at an interval of one second. The voltage and amperage for both the heaters is also noted down.

After this, the heat pipe assembly was disassembled at the cover plate and the base plate interface. The primary wick was completely removed off the substrate surface, collected and preserved for visual investigation. The substrate surface was wet-sanded using an 800-grit sandpaper to ensure removal of all the residual primary wick off the substrate surface. A thinner layer of nanofibers was used as the primary wick by laying it on the substrate surface. The heat pipe was put together the same way as mentioned earlier, and the experimental process repeated 5 times. 5 more trials were taken again but this time the evaporator chamber was completely void of the nanofibers as primary wicking material. This was done to allow collection of data for a case with bare substrate surface.

CHAPTER 7

RESULTS AND DISCUSSION

7.1. Optical observations

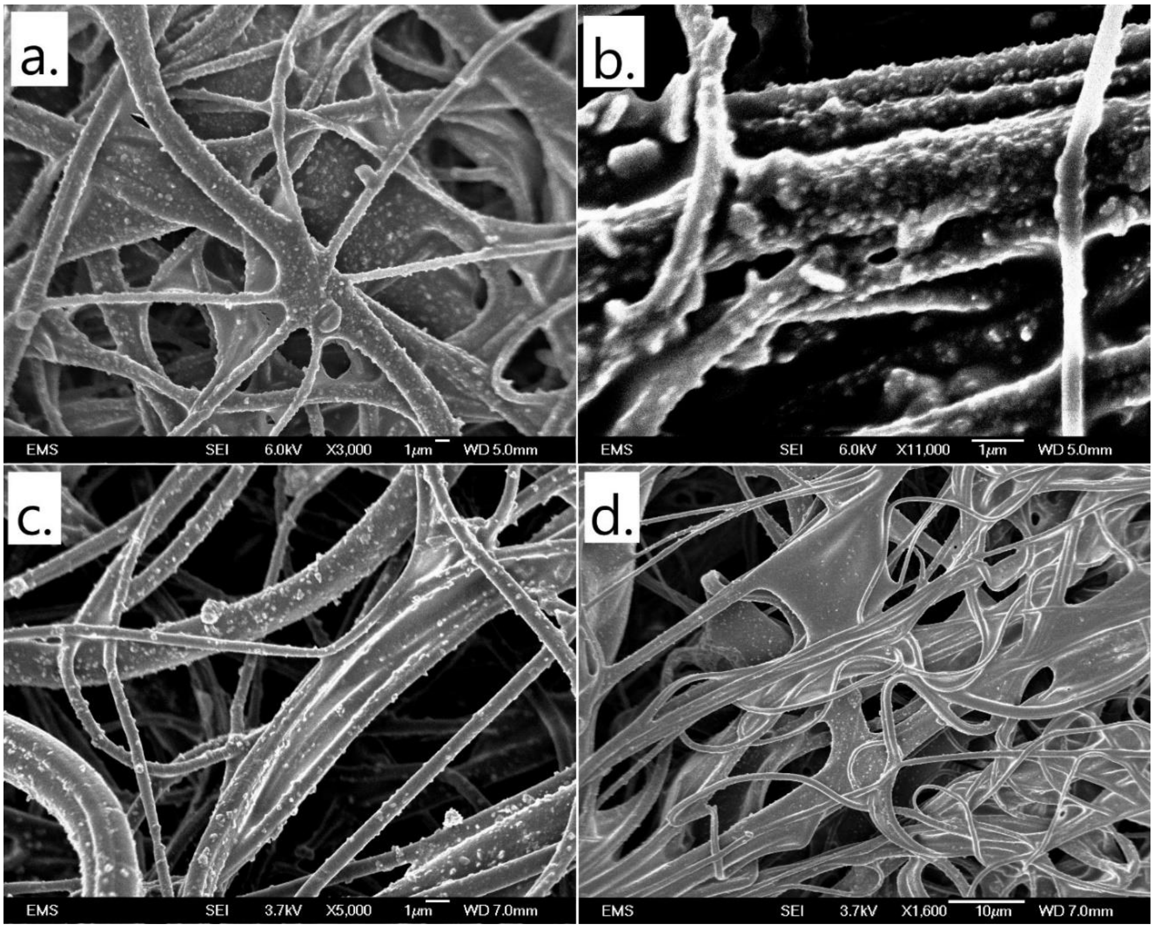

Figure 7.1 SEM images of solution blown PAN nanofibers magnified **a.** 3000 times, **b.** 11,000 times, **c.** 5,000 times, **d.** 1600 times

Ref. Fig.7.1 (a), (b), (c) and (d) show the SEM images of solution blown PAN nanofibers at different magnification levels. These images are taken post the trials on use of thick and thin layer of nanofiber mats as the primary wick. The diameter of nanofibers ranges between 200 nm to 500 nm. The pore size of the nanofiber mat is roughly 1 μm to 1.5 μm. It should be noted that the nanofiber deposition on the substrate surface leads to the formation of 3 dimensional bumps and valleys on the substrate surface. This increases the area of the substrate surface and aides in formation of new nucleation sites.

7.2 Theoretical and experimental flowrate comparison

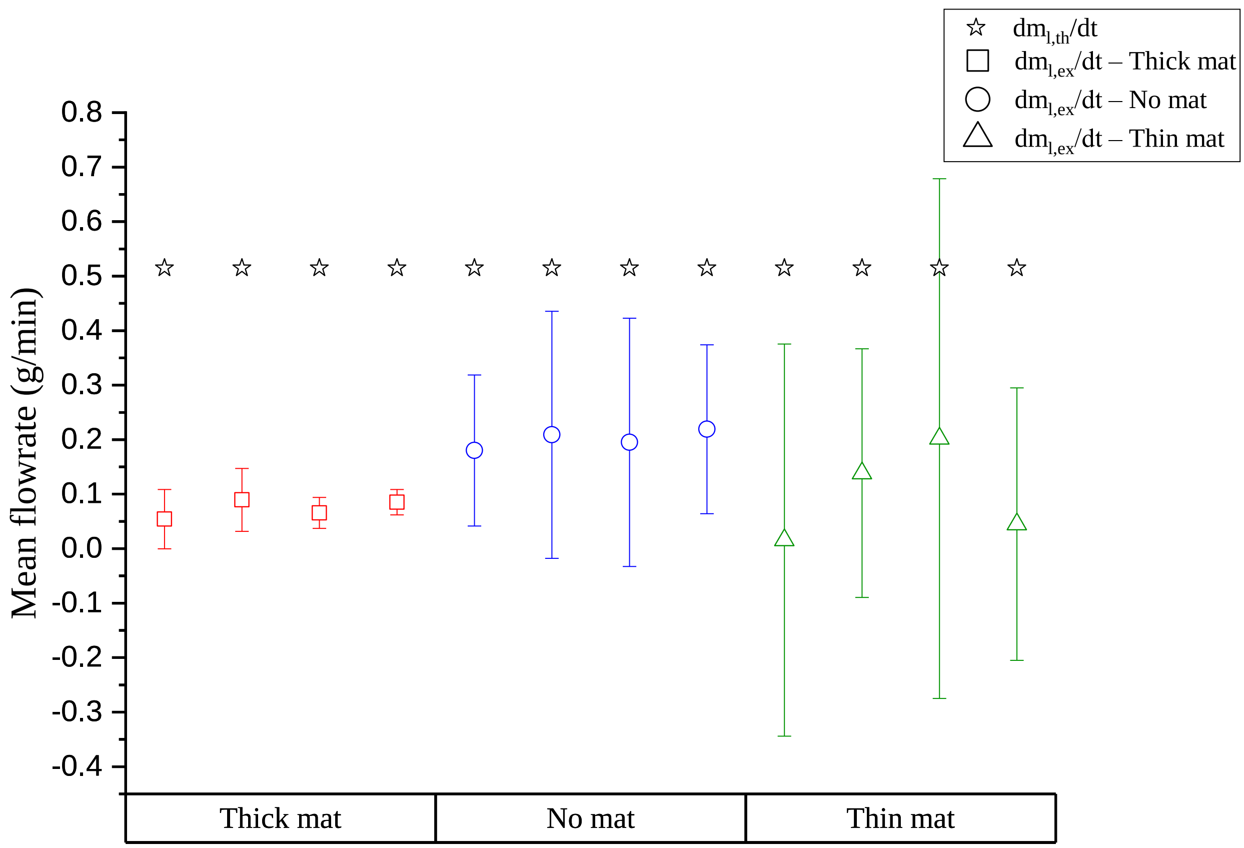

Figure 7.2 A comparative plot of the experimental as well theoretical plot of average mass flowrates during steady state for each of the trials. Measured and averaged experimental mass flowrate, $dm_{l,ex}/dt$ of the condensate in the heat pipe loop during steady state for each of the four trials for a case with no nanofibers, thin nanofibers and thick nanofibers are plotted side by side and clubbed together according to the case to allow for a case to case comparison. Theoretical mass flowrate, $dm_{l,th}/dt$ obtained by equation (13) considering no heat loss to the evaporator wall is also shown. Note that $dm_{l,ex}/dt$ and $dm_{l,th}/dt$ are given in grams per minute.

Ref. Fig. 7.2, a plot of the measured average experimental mass flowrate $dm_{l,ex}/dt$ for the condensate in the heat pipe loop, as well as the theoretical mass flowrate $dm_{l,th}/dt$ for the same is shown. The value of theoretical mass flowrate for flow through the loop at supplied heat, $q_i = 17.5$ W was estimated using equation (13). This value was found to be 0.515 g/min. Average experimental mass flowrate, $dm_{l,ex}/dt$ was calculated based on the flowrate measurements taken by the flowmeter and by plugging in those values in the following equation,

$$\frac{dm_{l,ex}}{dt} = \frac{dV_{l,ex}}{dt}\rho_l \tag{14}$$

where, $dm_{l,ex}/dt$ = experimental mass flowrate of condensate in the loop given in (g/min); $dV_{l,ex}/dt$ = volumetric flowrate of the condensate measured using the flowmeter in (cm^3/min) and $\rho_l =$ density of the condensate, which is nothing but the density of DI water = 1 g/cm^3.

Consider the $dm_{l,ex}/dt$ plots in case of thick nanofiber mat as the primary wick in Ref. Fig. 7.2. A good repeatability is seen for the four individual cases with the mean value of $dm_{l,ex}/dt$ lying around 0.07 g/min. The error bars are also close to the mean indicating a low standard error. However, $dm_{l,ex}/dt$ value is very much less than that of $dm_{l,th}/dt$ which was found to be 0.515 g/min.

Ref. Fig. 7.2. also shows the $dm_{l,ex}/dt$ plots in case of no nanofiber mat as primary wick. Repeatable result is seen for the four individual cases with the mean value of $dm_{l,ex}/dt$ lying around 0.2 g/min. The error bars are a farther away from the mean as compared to the earlier case indicating a higher fluctuation in the mass flowrate. However, $dm_{l,ex}/dt$ value is closer to that of $dm_{l,th}/dt$ which was found to be 0.515 g/min.

Similarly, $dm_{l,ex}/dt$ for a case with thin nanofiber mat are also plotted on the graph Ref. Fig. 7.2. The mean $dm_{l,ex}/dt$ is around a value of 0.1 g/min. This value is closer to $dm_{l,th}/dt$ as compared to the case with thick nanofibers as the primary wick but farther away as compared to the case with no nanofiber mat as the primary wick. Also note that the error bars for each of the four trials for this case are farther away from the previous two cases indicating a tremendously fluctuating mass flowrate.

7.3 Temperature and heat flux measurements

One dimensional heat flux is considered perpendicular to the cross section of the aluminum block assuming the heat losses in the rest of the dimensions to be negligible. This is because the thermal conductivities of both PEEK and PTFE insulation are very less than that of aluminum $k_{PEEK} = k_{PTFE} = 10^{-3} k_{al}$ where k_{PEEK}, k_{PTFE} and k_{al} are the thermal conductivity coefficients for PEEK, PTFE and aluminum respectively. Heat flux passing through the aluminum block was accounted for using three different methods which were as follows: Heat flux measured based on the input power, heat flux measured based on the temperature of thermocouples inserted inside the aluminum block, heat flux measured based on the flowrate of water flowing through the flowmeter. As mentioned earlier, the potential difference, *P* and current, *C* passing through the primary heater were measured and noted down. The input power, q_i was calculated using the expression,

$$q_i = P \times C \tag{15}$$

where, $P =$ Potential difference measured in Volts and $C =$ current measured in Amperes the heat flux based on input power is calculated by the following formula:

$$q_i'' = \frac{q_i}{S} \tag{16}$$

Where q_i is the input power given in Watts and S is the cross sectional area of the aluminum block taken in cm^2

4 T-type thermocouples were used to measure the temperature along the vertical axis of the aluminum block. The thermocouple closest to the heater was named T_1 followed by T_2 and so on for T_3 and T_4. Heat fluxes between each of those were measured using the Fourier's law:

$$q_{t,ex}'' = k_{al}\frac{dT_{ex}}{dx} \tag{17}$$

where, $q_{t,ex}''$ is experimental thermocouple based heat flux calculated in W/cm^2; the thermal conductivity of aluminum, k_{al} = 2.05 W/(cm°C) and dT_{ex}/dx is the temperature gradient measured along the vertical axis of the aluminum block measured in (°C/cm). The experimental surface temperature can also be extrapolated using the thermocouple temperature values. The temperature gradient was averaged over the distance between the thermocouple T_4 and the experimental substrate surface for which the surface temperature $T_{surf,ex}$ was given in °C

$$T_{surf,ex} = T_4 - \left(\frac{dT_{ex}}{dx}\right)_{average} \triangle x \tag{18}$$

Where $(dT/dx)_{average}$ is the temperature gradient taken in (°C/cm) and $\triangle x$ is the distance between the substrate surface and T_4 taken in cm.

The experimental heat flux based on flowrate of water is calculated by the following formula.

$$q_{f,ex}'' = I\frac{dm_{l,ex}}{dt} \tag{19}$$

where, latent heat of vaporization of water, I = 2×10^3 J/g and the experimental mass flowrate $dm_{l,ex}/dt$ based on the flowmeter readings, $dV_{l,ex}/dt$ is calculated using the equation (14). A total of 12 trials were taken. The performance of nanofibers in the heat pipe was analyzed during the steady state. 4 trials were taken using a thin nanofiber mat, 4 using a thick nanofiber mat and 4 more without any nanofibers on the substrate surface.

Consider the heat pipe in a steady state. Heat is supplied to the working fluid contained in the primary wick through the substrate surface. The working fluid absorbs the latent heat of vaporization and evaporates. By doing that, the vapor volume also expands applying a positive pressure on the walls of evaporator. At the same point of time the same amount of working fluid which has previously evaporated and moved towards the condenser, condenses in the condenser leading to a volume decrease accompanied by a negative pressure inside the condenser. Thus, drawing of the vapor mass from the evaporator towards the condenser is facilitated because of the pressure difference. This is also accompanied by a new batch of liquid mass to be drawn inside the evaporator chamber via the secondary wick which also allows for a regulated amount of fluid flow towards the evaporator. The secondary wick is covered in PAN nanofibers which have a high enough capillary pressure which prohibits the reverse movement of vapor from the evaporator chamber to the compensation chamber.

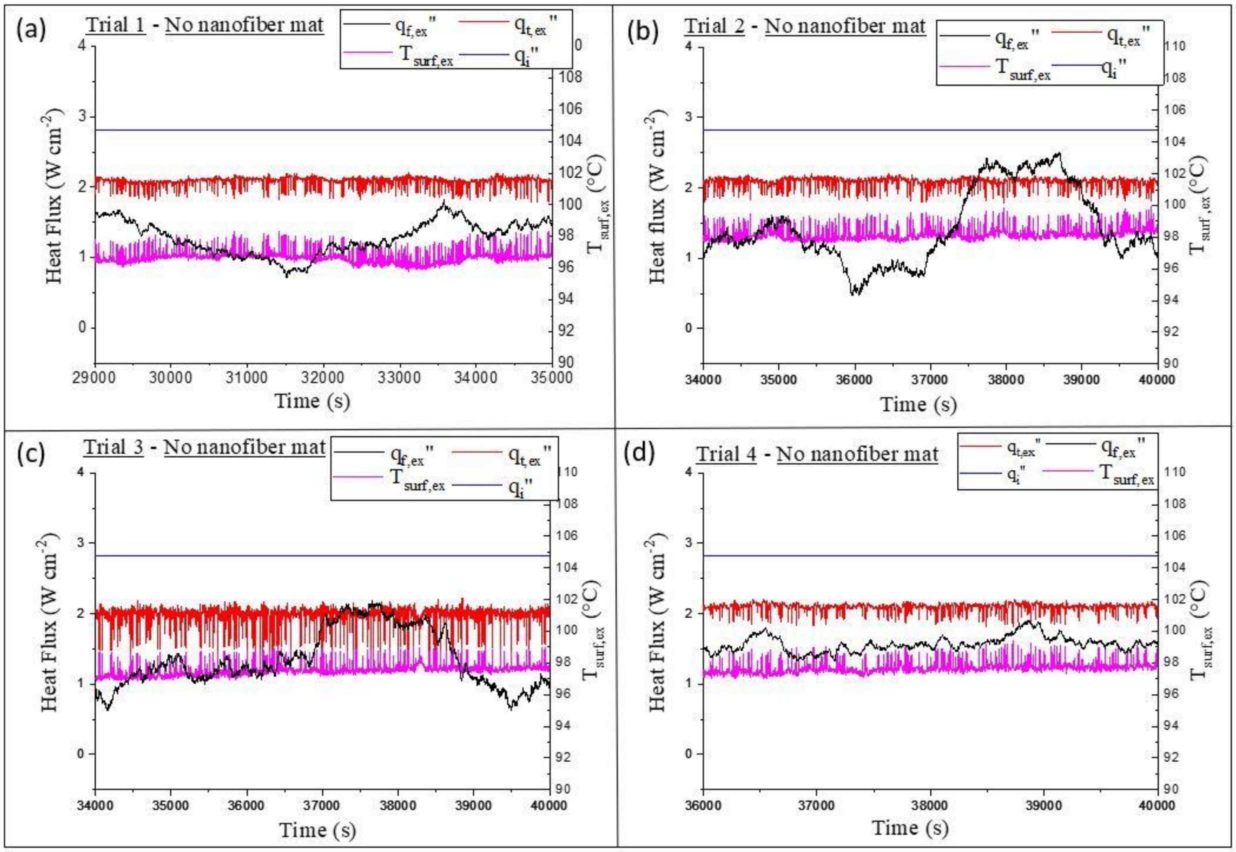

Figure 7.3 Time versus heat flux and substrate surface temperature plot of the trials with no nanofibers on the substrate surface under steady state conditions. a, b, c, and d represent the respective plots for trials 1, 2, 3 and 4 for a case with no nanofibers on the substrate surface.

Ref. Fig. 7.3 shows a time versus heat flux and surface temperature plot of the case with no nanofibers as the primary wick. Equation (15) to Equation (19) were used to calculate the values, q_i'' $q_{t,ex}''$, $T_{surf,ex}$, and $q_{f,ex}''$ respectively. The $q_{f,ex}''$ is a moving average curve of the heat flux based on the mass flowrate of water $dm_{l,ex}/dt$ over a time interval of 1800 sec. The input heat supplied, q_i was kept constant throughout the course of a trial at 17.5 W. As seen from the plot, the system is in steady state as the temperature of the substrate surface, $T_{surf,ex}$ remains constant over the course of time. Some spikes are also seen on the surface temperature $T_{surf,ex}$ curve as well as the heat flux $q_{t,ex}''$ curve based on the thermocouple readings indicating that the nature of flow of water in the evaporator chamber itself was fluctuating locally even though the net flowrate, $dm_{l,ex}/dt$ was positive and unidirectional. There is a significant difference of 0.8 W/cm^2 between q_i'' and $q_{t,ex}''$ which is an indicator of the heat losses through the insulation. There is also a significant difference between q_i'' and $q_{f,ex}''$ although at some points, there is an intersection between the two. This is an indicator that there are considerable flow losses within the heat pipe loop. It can also be because enough fluid is not able to flow due to resistance by the secondary wick. The mass flowrate of water is also fluctuating in nature. This can be explained by the continuous expansion and contraction of the working fluid inside the evaporator chamber. A good repeatability is seen in the values for q_i'' and $q_{t,ex}''$ when comparing all the four cases with each other. The heat flux based on the flowrate of the working fluid condensate, $q_{f,ex}''$ however, has a fluctuating nature.

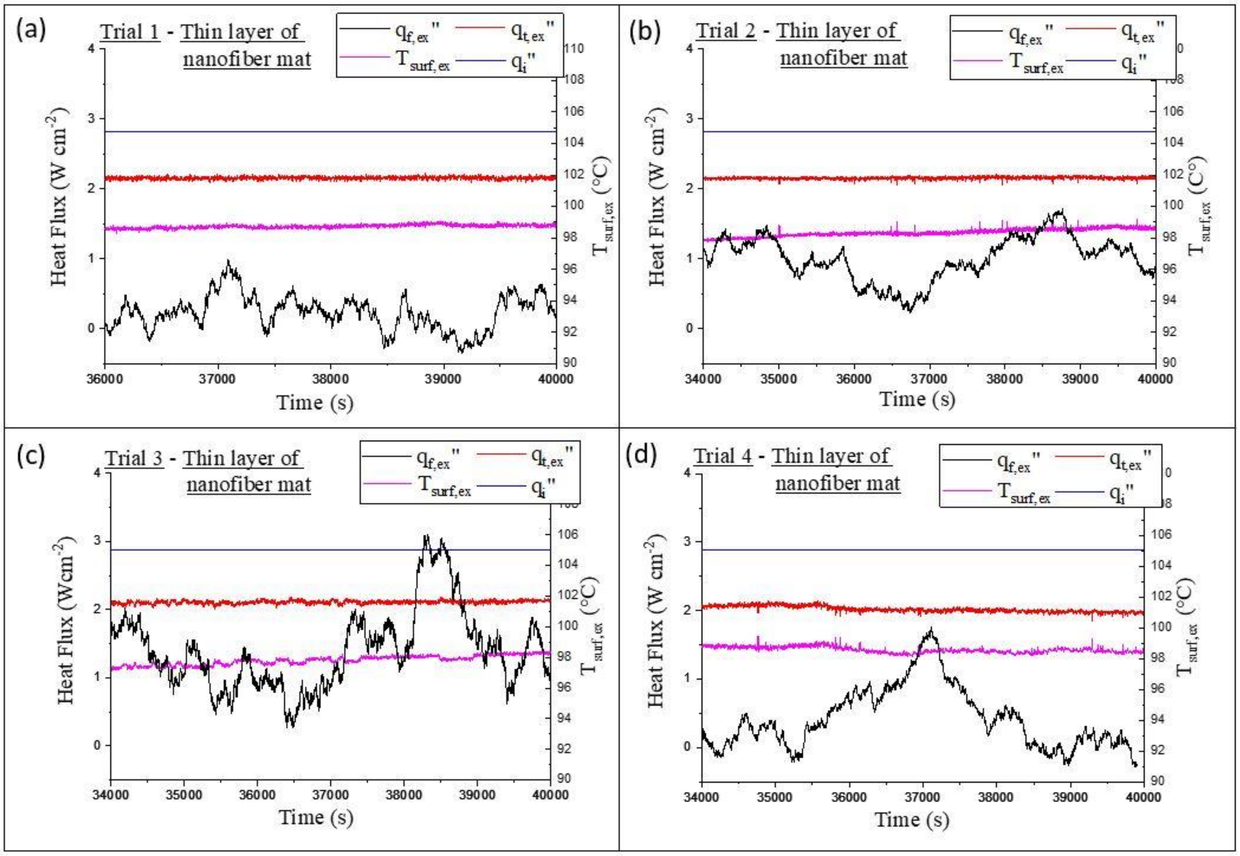

Figure 7.4 Time versus heat flux and substrate surface temperature plot of the trials with a thin layer of nanofiber mat on the substrate surface under steady state conditions. a, b, c, and d represent the respective plots for trials 1, 2, 3 and 4 for a case with a thin layer of nanofiber mat on the substrate surface.

Following the trials with no nanofiber mat as primary wick, a very thin layer of PAN nanofiber mat was placed on the substrate surface. Ref. Fig. 7.4 shows heat flux and substrate temperature plots of the four cases with a thin layer of nanofiber mat on the substrate surface when the system is in steady state. Identical to the case of no nanofiber mat in the evaporator, the supplied input heat, q_i was kept constant throughout the course of experiment at 17.5 W. Equation (15) to equation (19) were used to calculate the values of q_i'', $q_{t,ex}''$, $T_{surf,ex}$, and $q_{f,ex}''$ respectively. A difference of about 0.7 W/cm^2 between q_i'' and $q_{t,ex}''$ is an indicator of heat losses through the insulation. The $q_{f,ex}"$ values were calculated by taking a moving average of the flowmeter readings, over a span of 1800 seconds. Similar to the previous case, the mass flowrate, $dm_{l,ex}/dt$ is positive and unidirectional as indicated by the moving average curve of $q_{f,ex}"$.

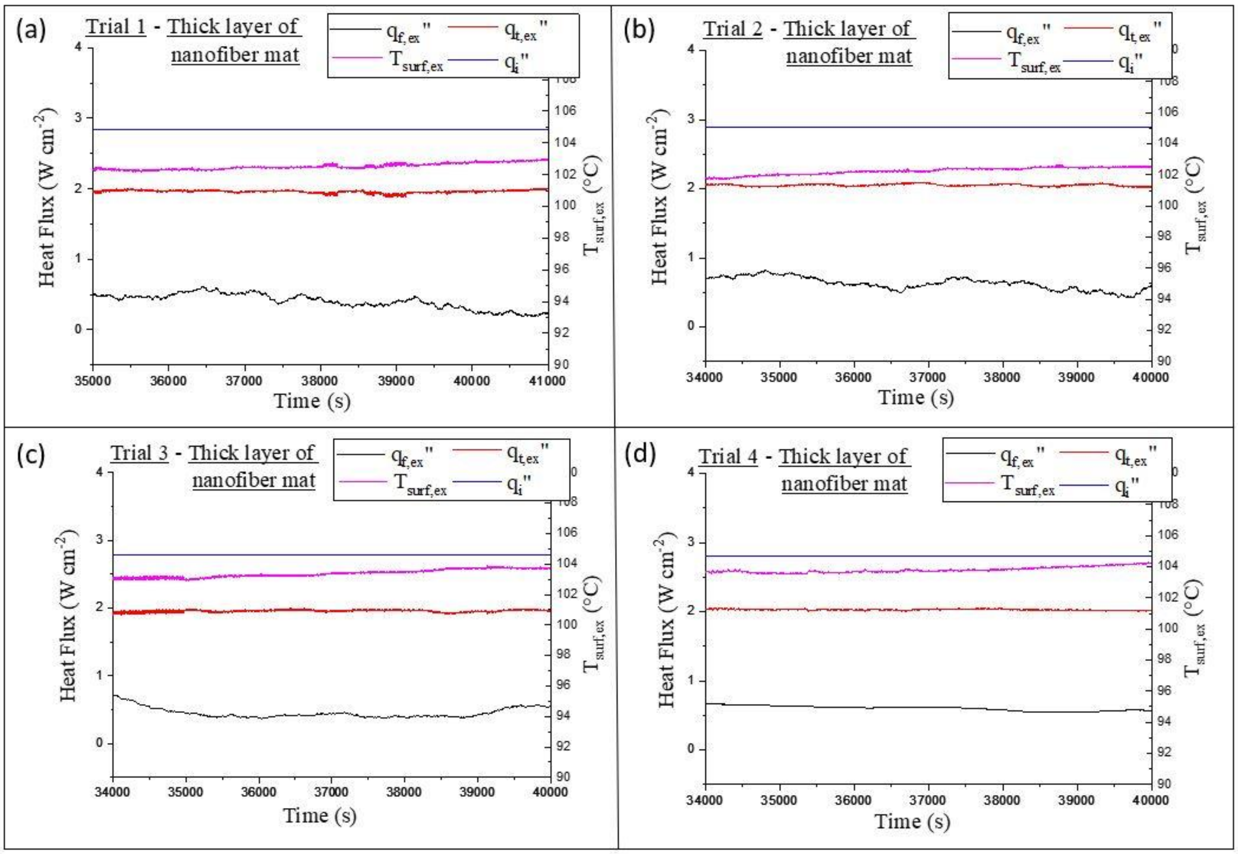

Figure 7.5 Time versus heat flux and substrate surface temperature plot of the trials with a thick layer of nanofiber mat in the evaporator under steady state conditions. a, b, c, and d represent the respective plots for trials 1, 2, 3 and 4 for a case with a thick layer of nanofiber mat on the substrate surface.

Ref. Fig. 7.5, similar to the previous plots, time versus heat flux plots of four trials with thick layer of nanofiber mat are shown. Equations (15) to equation (19) are used to calculate the values of $q_i"$ $q_{t,ex}"$, $T_{surf,ex}$, and $q_{f,ex}"$ respectively. A difference of 0.7 W/cm^2 is seen between the values of $q_i"$ and $q_{t,ex}"$ respectively. The heat loses in the insulation are evident and very much comply with those seen in the cases before. The values for $q_{f,ex}"$ are quasi steady which indicates that the mass flowrate, $dm_{l,ex}/dt$ in the system was positive and unidirectional.

The substrate surface temperature, $T_{surf,ex}$ in Ref. Fig. 7.3 which is the case of four trials with no nanofiber mat as the primary wick has a rapid rising and falling nature which is an indicator that the substrate surface is getting heated and cooled rapidly. This could mean that there is a rapid film formation instantly followed by its breakage on the substrate surface. When a film of vapor starts forming on the substrate surface, the heat flux $q_{t,ex}"$, falls relatively as a result of which the surface temperature, $T_{surf,ex}$ rises as long as the film is present and growing over the surface. After a certain while the film collapses due to incoming fluid form the compensation chamber via the secondary wick. This causes a miniature local flooding in the evaporator chamber for that time instant. This results in the surface temperature, $T_{surf,ex}$ to drop rapidly and a corresponding rise in $q_{t,ex}"$. This rise and fall of the substrate surface temperature $T_{surf,ex}$ is validated by the corresponding rise and fall in $q_{t,ex}"$.

The substrate surface temperature, $T_{surf,ex}$ in Ref. Fig. 7.4 which is the case of four trials with thin nanofiber mat as the primary wick also has a rising and falling nature but it is a smoother curve as compared to that of the case with no nanofibers on the substrate surface in Ref. Fig. 7.3 which is an indicator that the substrate surface temperature, $T_{surf,ex}$ in case with thin nanofiber mat as the primary wick is more uniform in nature. This could mean that the working fluid in liquid form is more uniformly distributed on the substrate surface as compared to the previous case. The nanofibers help to disperse the liquid more uniformly over the substrate surface thus reducing the possibility of film formation and breakage. Thus, even in case of a miniature local flooding in the evaporator chamber, the liquid working fluid is evenly pumped all over the surface due to the capillary pumping offered by the thin layer of nanofiber mat. This results in the surface temperature, $T_{surf,ex}$ to remain more uniform and a corresponding uniformity in $q_{t,ex}''$.

The substrate surface temperature, $T_{surf,ex}$ in Ref. Fig. 7.5 which is the case of four trials with thick nanofiber mat as the primary wick does not have a rising and falling nature and is an even smoother curve as compared to the both of previous cases with no nanofibers on the substrate surface in Ref. Fig. 7.3 as well as thin nanofiber layer mat on the substrate surface in Ref. Fig. 7.4 This is an indicator that the substrate surface temperature, $T_{surf,ex}$ in case with thick nanofiber mat as the primary wick is more uniform in nature compared to the other two cases. This indicates that a more uniform distribution of the liquid working fluid on the substrate surface as compared to the previous case holds true. A thicker nanofiber mat facilitates a higher capillary pumping of the fluid and its dispersion over the substrate surface. As a result of this, the substrate temperature, $T_{surf,ex}$ is also uniform with the corresponding $q_{t,ex}''$ being equally uniform.

Note also the $q_{f,ex}''$ curve in Ref. Fig. 7.3. This value fluctuates a lot which is an indicator of the fluctuating mass flowrate of condensate of the working fluid $dm_{l,ex}/dt$ in the heat pipe loop. These fluctuations are also evident by the distant error bars from the mean $dm_{l,ex}/dt$ for all the four cases with no nanofibers as the primary wick in Ref. Fig 7.2. Note the $q_{f,ex}''$ curve in Ref. Fig. 7.4. This value is also fluctuating indicating the fluctuations in mass flowrate of water $dm_{l,ex}/dt$ even with a thin layer of nanofiber mat as the primary wick on the substrate surface. The error bars for these fluctuations are farther away from the mean $dm_{l,ex}/dt$ as indicated in Ref. Fig

7.2 which tells us that the fluctuations have a higher magnitude in a case with thin nanofibers mat as the primary wick as compared to a case of no nanofiber mat as the primary wick. Note also the $q_{f,ex}''$ curve in Ref. Fig. 7.5 This curve is more linear as compared to the previous two cases indicating a uniformity in mass flowrate of water $dm_{l,ex}/dt$ in the loop. This lower magnitude of fluctuations is also evident from the shorter error bars for mean mass flowrate $dm_{l,ex}/dt$ for all the four cases of thick nanofiber mat as the primary wick on the substrate surface in Ref. Fig. 7.2. This is a good indicator that the nanofibers also assist in attaining a uniform and unidirectional net flowrate in the heat pipe loop.

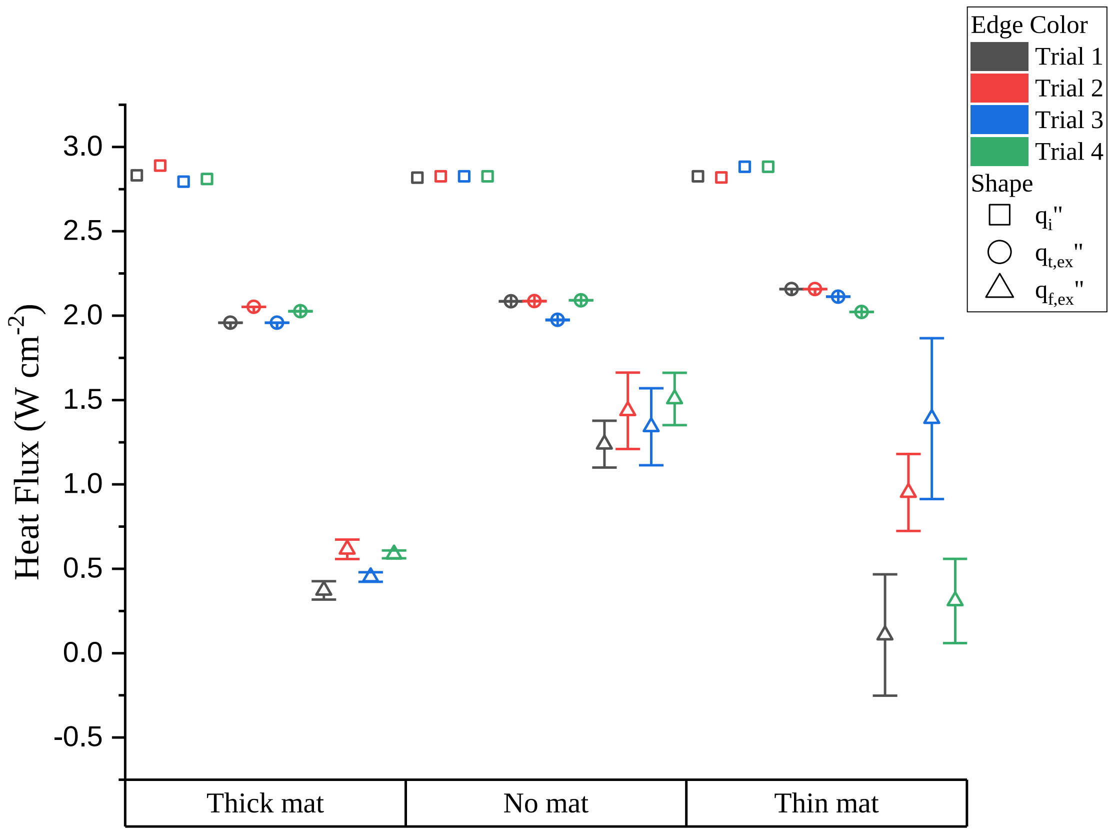

Figure 7.6 A compilation of the average of the heat flux values for each of the individual trials. The mean and standard deviation for all the trials was calculated. This was followed by standard error calculations for each of the 12 trials. The X-axis is divided in 3 sections i.e., Thick nanofiber mat, no nanofiber mat and thin nanofiber mat. The Y-axis represents magnitude of average of the heat fluxes, q_i'' , $q_{t,ex}''$, and $q_{f,ex}''$ along with standard error estimated from equations (15) to equation (19). The outline color of the symbols represents the trial number for each of the cases. The shape of symbol represents the individual type of heat flux measured.

Ref. Fig. 7.3, Fig. 7.4 and Fig. 7.5. Consider the curves and mean values for the heat flux based on input, q_i'' and the heat flux based on thermocouple readings, $q_{t,ex}''$. These are identical in all the cases with a mean deviation of 0.2 W/cm^2 to 0.4 W/cm^2 for all the trials. This indicates that $q_{t,ex}"$ is repeatable and almost the same for all the trials. Mean and standard error for all $q_i"$, $q_{t,ex}"$ and $q_{f,ex}"$ for each of the 12 trials is also shown in Ref. Fig. 7.6. As indicated, the heat flux based on the thermocouple readings, $q_{t,ex}"$ is almost the same in all the cases of no nanofiber mat, thin layer of nanofiber mat and a thick layer of nanofiber mat. Note also that the mean of all $q_{f,ex}"$ is less than the mean of all the respective $q_i"$ and $q_{t,ex}"$. This means that the secondary wick provided a considerable resistance to the mass flow of working fluid.

Ref. Fig. 7.6 the mean of $q_{f,ex}"$ for all the four cases with thick layer of nanofiber mat is almost constant and lies around a value of 0.5 W/cm^2. However, $q_{f,ex}"$ is higher in the case of no nanofiber mat as compared to $q_{f,ex}"$ of thick layer of nanofiber mat case. This means that the thicker layer of nanofiber mat is does not help with enhancing heat transfer, but rather hinders it. The $q_{f,ex}"$ for case with thin layer of nanofibers is very widespread along the Y axis of Ref. Fig. 7.6 which is why its nature cannot be determined. However, $q_{f,ex}"$ for Trial 3 of the case with thin layer of nanofiber mat which is the highest $q_{f,ex}"$ for all of the cases with thin layer of nanofiber mat is almost identical to the values of $q_{f,ex}"$ for trials with no nanofiber mat on the substrate surface. More trials for a case of thin layer of nanofiber mat would be necessary to truly determine its nature and if the $q_{f,ex}"$ is repeatable or not.

Ref. Fig. 7.6 now consider the respective errors of $q_{f,ex}"$ for all the trials. Standard error for $q_{f,ex}"$ of a thick layer of nanofiber mat is closest to the mean as compared to that of the $q_{f,ex}"$ for all the cases of no nanofiber mat as well as $q_{f,ex}"$ for all the cases of thin layer of nanofiber mat. A similar trend is seen in Ref. Fig 7.2 where the error bars for the $dm_{l,ex}/dt$ of thicker layer of nanofiber mat are closer to the mean as compared to that of a thin layer of nanofiber mat as well as no nanofiber mat as the primary wick. This means that a thick layer of nanofiber mat assists in getting a more uniform flowrate owing to its high capillary action.

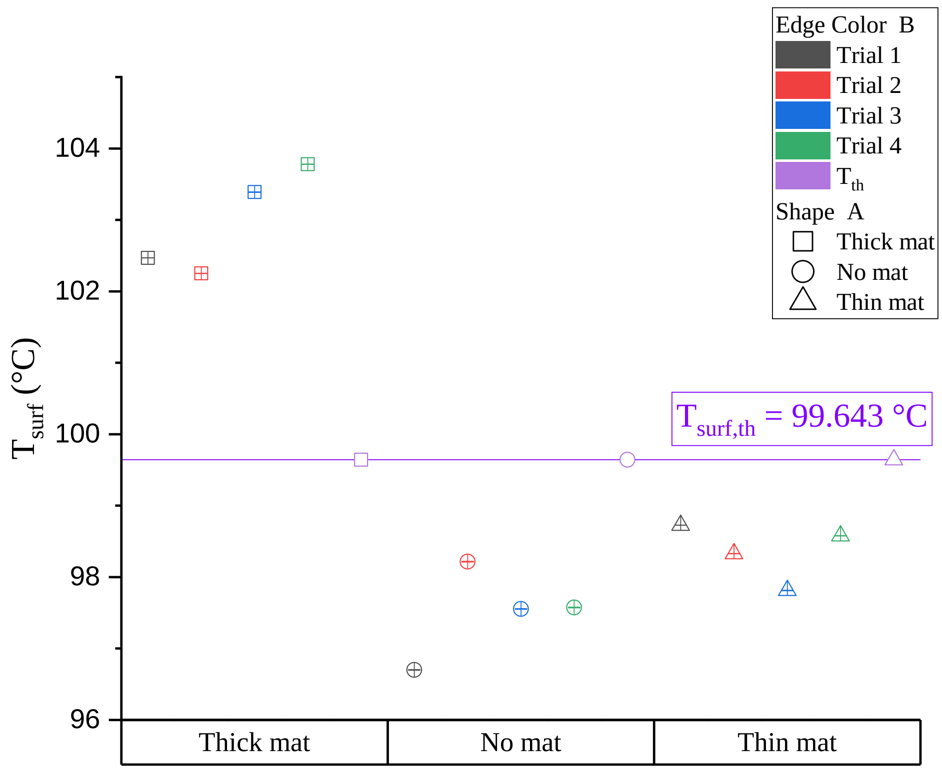

Figure 7.7 A compilation of averaged $T_{surf,ex}$ values for each trial. The mean and standard deviation for all the trials was calculated. This was followed by standard error calculations for each of the 12 trials. The X-axis is divided in 3 sections i.e., thick nanofiber mat, no nanofiber mat and thin nanofiber mat. The Y-axis represents magnitude of average of the heat flux along with standard error estimated from equation (15) to equation (19). The outline color of the symbols represents the trial number for each of the cases. The shape of symbol represents the type of heat flux measured. Theoretical temperature, $T_{surf,th}$ in steady state found by solving equation (9) and equation (11) is also shown.

Ref. Fig. 7.7 it can be seen form the plot that the values $T_{surf,ex}$ for all the trials of thick layer of nanofiber mat case was higher than the trials with no nanofiber mat as well as the case with thin layer of nanofiber mat as the primary wick. This indicates that the thick layer of nanofiber mat did not help for cooling of the substrate surface but rather worsened it. Also, the values of $T_{surf,ex}$ for a case with thin layer of nanofiber mat were close to the $T_{surf,ex}$ values for a case with no nanofiber mat but slightly higher. This indicated that reducing the thickness of nanofiber mat makes the heat transfer conditions better but does not help with improving the heat transfer in comparison to that over a bare surface.

$T_{surf,th}$, the theoretical substrate surface temperature which was found by solving equation (9) and equation (11) is also shown in Ref. Fig. 7.7. $T_{surf,ex}$ is relatively higher than $T_{surf,th}$ in the case with a thick layer of nanofiber mat on the substrate surface. This indicates that a thick layer of nanofiber mat does not help with cooling, but it rather ends up causing the substrate surface temperature to rise significantly.

The theoretical substrate surface temperature, $T_{surf,th}$ on the other hand was relatively lower than $T_{surf,ex}$ in the case with a thick layer of nanofiber mat on the substrate surface as well as no nanofiber mat on the substrate surface. This indicates that a thinner layer of nanofiber mat is more beneficial when it comes to cooling of the substrate surface as compared to its thicker counterpart. Regardless, $T_{surf,ex}$ for the cases with a thinner layer of nanofibers was slightly higher than $T_{surf,ex}$ for all the cases with no nanofiber mat as primary wick on the substrate surface indicating that nanofibers prove as a resistance to the heat transfer on the surface.

CHAPTER 8

CONCLUSIONS

Use of nanofibers as wicking material in an LHP was studied. Three cases each with four trials for repeatability were compared to each other namely no nanofibers as the primary wick, a thin layer of nanofibers as the primary wick and a thick layer of nanofibers as the primary wick. Their performance was evaluated based on comparison of the respective heat transfer capabilities which was analyzed by measuring and comparing the heat flux based on supplied heat input, q_i''; heat flux based on thermocouple temperature readings, $q_{t,ex}''$ and heat flux based on mass flowrate of working fluid condensate in the heat pipe loop, $q_{f,ex}''$. The input heat flux q_i'' was kept constant and the heat flux based on thermocouple readings, $q_{t,ex}''$ was found to be repeatable and the same for all the three cases of no nanofiber mat as the primary wick and thin layer and a thick layer of nanofiber mat as the primary wick. Significant insulation losses were noted as the value of $q_{t,ex}''$ for all the trials differ with a magnitude of 0.2 W/cm^2 to 0.4 W/cm^2 q_i'' for all the trials. Heat flux based on mass flowrate of water, $q_{f,ex}''$ however, was repeatable for the case with a thicker layer of nanofiber mat on the substrate surface but was highly fluctuating and less repeatable for the case of thin layer of nanofiber mat as well as the case of no nanofiber mat as the primary wick. This can be caused by a more uniform and continuous capillary pumping of the working fluid by a thicker layer of nanofiber mat in comparison to a thinner layer and no nanofiber mat.

A theory to estimate the theoretical mass flowrate, $dm_{l,th}/dt$ was also developed. This estimate was compared the experimental mass flowrate, $dm_{l,ex}/dt$ for each of the three cases. The mass flowrate measured experimentally in all the cases was significantly lower than that of the theoretical mass flowrate. This could be explained by the flow losses of the working fluid in the heat pipe loop.

Based on the results obtained, it is clear that using the nanofibers does not aid in improving the heat transfer rate but rather hinders the heat transfer. A thick layer of nanofiber mat on the substrate surface helps in making the flowrate steady owing to its high capillary action but at the same point of time causes a resistance to the heat transfer rate. Using a thinner layer of nanofibers does improve the heat transfer in comparison to its thicker counterpart but it does not improve the heat transfer better than the case with no nanofibers.

As for the future scope for the experiment, a working fluid other than DI water can be used to test its performance and effect. Also, more trials can be taken for the case with thin nanofiber mat to study the $q_{f,ex}''$ better. Nanofibers made of other materials can also be used and different nanofiber and working fluid combinations can be tried to test their performance.

CITED LITERATIRE

An. S., Kim Y., Lee M., Yarin A. L., Sam S. Yoon (2017). “Wetting and Coalescence of Drops of Self-Healing Agents on Electrospun Nanofiber Mats”, *Langmuir*, 33, 10663−10672

Carey V. P. (2007). “*Liquid Vapor Phase Change Phenomena: An Introduction to the Thermophysics of Vaporization and Condensation Processes in Heat Transfer Equipment, Second Edition*”, Boca Raton : Chapman and Hall/CRC, 2018.

Dong L., Quan X., Cheng P. (2014), “An experimental investigation of enhanced pool boiling heat transfer from surfaces with micro/nano-structures”, *International Journal of Heat and Mass Transfer,* Volume 71, Pages 189-196

Fischer S., Sahu R. P., Sinha-Ray S., Yarin A. L., Gambaryan-Roisman T., Stephan P. (2017), “Effect of nano-textured heater surfaces on evaporation at a single meniscus”, *International Journal of Heat and Mass Transfer,* Volume 108, Part B, Pages 2444-2450

Freystein M., Kolberg F., Spiegel L. , Sinha-Ray S., Sahu R. P., Yarin A. L., Gambaryan-Roisman T. , Stephan P. (2014), “Trains of taylor bubble over hot nanotextures mini channel surface”, *International Journal of Heat and Mass Transfer,* Volume 93, Pages 827-833

Ji X., Wang Y., Xu J., Huang Y. (2017), “Experimental study of heat transfer and start-up of loop heat pipe with multiscale porous wicks”, *Applied Thermal Engineering*, Volume 117, Pages 782-798

Jo H. S., An S., Nguyen X. H., Kim Y. I., Bang B., James S.C., Choi J, Yoon S. S. (2018), "Modifying capillary pressure and boiling regime of micro-porous wicks textured with graphene oxide", *Applied Thermal Engineering*, Volume 128, Pages 1605-1610

Khalili M., Shafii M. B. (2016), “Experimental and numerical investigation of the thermal performance of a novel sintered-wick heat pipe.”, *Applied Thermal Engineering*, Volume 94, Pages 59-75

Lembach A., Tan H., Roisman I., Gambaryan-Roisman T., Zhang Y., Tropea C., Yarin A. L. (2010), “Drop impact spreading splashing and penetration into nanofiber mats”, *Langmuir*, 26(12), 9516–9523

Li H., Zhou B., Tang Y., Zhou R., Liu Z., Xie Y. (2017), “Effect of working fluid on heat transfer performance of the anti-gravity loop-shaped heat pipe”, *Applied Thermal Engineering*, Volume 88, 5 September 2015, Pages 391-397

Ling W., Zhou W., Yu W., Liu R., Hui K.S. (2017), “Thermal performance of loop heat pipes with smooth and rough porous copper fiber sintered sheets”, *Energy Conversion and Management*, Volume 153, Pages 323-334

Putra N., Ramadhan R. S., Septiadi W. N., Sutiarso (2015) “Visualization of the boiling phenomenon inside a heat pipe using neutron radiography”, *Experimental Thermal and Fluid Science*, Volume 66, Pages 13-27

Rabiee R., Rajabloo B., Désilets M., Proulx P. (2019) “Heat transfer analysis of boiling and condensation inside a horizontal heat pipe”, *International Journal of Heat and Mass Transfer* Volume 139, Pages 526-536

Reay D., McGlen R., and Kew P. (2013) *“Heat Pipes: Theory, Design and Applications”*, Kidlington, Oxford, UK : Butterworth-Heinemann, an imprint of Elsevier, 2014.

S. Sinha-Ray, Y. Zhang, A. L. Yarin (2011) “Thorny Devil Nanotextured Fibers: The Way to Cooling Rates on the Order of 1 kWcm-2”, *Langmuir*, 27(1), 215–226

Sahu R. P., Sinha-Ray S., Sinha-Ray S., Yarin A. L. (2016), “Pool boiling of Novec 7300 and self-rewetting fluids on electrically-assisted supersonically solution-blown, copper-plated nanofibers”, *International Journal of Heat and Mass Transfer,* Volume 95, Pages 83-93

Sahu R. P., Sinha-Ray S., Sinha-Ray S., Yarin A. L. (2015), “Pool boiling on nano textured surfaces comprised of electrically assisted supersonically solution blown copper plated nanofibers”, *International Journal of Heat and Mass Transfer*, Volume 87, Pages 521-535

Sankaran A., Zhang W., Yarin A. L. (2018), “Pool boiling in deep and shallow vessels”, *International Journal of Heat and Mass Transfer,* Volume 127, Part C, Pages 857-866

Sinha-Ray S., Yarin A. L. (2014), “Drop impact cooling enhancement on nano-textured surfaces. Part I: Theory and results of the ground (1 g) experiments”, *International Journal of Heat and Mass Transfer,* Volume 70, Pages 1095-1106

Sinha-Ray S., Sinha-Ray S., Yarin A. L., Weickgenannt C. M., Emmert J., Tropea C. (2013) Drop impact cooling enhancement on nano-textured surfaces. Part II: Results of the parabolic flight experiments [zero gravity (0g) and supergravity (1.8g)], *International Journal of Heat and Mass Transfer*, Volume 70, Pages 1107-1114

Sinha-Ray S., Yarin A.L., Pourdeyhimi B. (2010), “The production of 100/400 nm inner/outer diameter carbon tubes by solution blowing and carbonization of core–shell nanofibers”, *Carbon* Volume 48, Issue 12, Pages 3575-3578

Sinha-Ray S., Zhang W., Sahu R. P., Sinha-Ray S., Yarin A. L. (2017) “Pool boiling of Novec 7300 and DI water on nano-textured heater, covered with supersonically-blown or electrospun polymer nanofibers*”, International Journal of Heat and Mass Transfer*, Volume 106, Pages 482-490

Sinha-Ray S., Zhang W., Stoltz B., Sahu R. P., Sinha-Ray S., Yarin A. L. (2017), "Swing-like pool boiling on nano-textured surfaces for microgravity applications related to cooling of high-power microelectronics", *Microgravity,* Volume 3, Issue 1, Page 9 (2017)

Srikar R., Gambaryan-Roisman T., Steffes C., Stephan P., Tropea C., Yarin A. L. (2009), "Nanofiber coating of surfaces for intensification of drop or spray impact cooling", *International Journal of Heat and Mass Transfer,* Volume 52, Issues 25–26, Pages 5814-5826

Tharayil T., Asirvatham L. G., Ravindran V., Wongwises S. (2016), "Effect of filling ratio on the performance of a novel miniature loop heat pipe having different diameter transport lines", *Applied Thermal Engineering*, Volume 106, Pages 588-600

Wang D., Wang X., Zhou P., Wu Z., Duan B., Wang C. (2014), "Influence of packing density on performance of porous wick for LHP", *Powder Technology*, Volume 258, Pages 6-10

Wang X., Wei J., Deng Y., Wu Z., Sundén B. (2018), "Enhancement of loop heat pipe performance with the application of micro nano hybrid structures", *International Journal of Heat and Mass Transfer, Volume 127*, Part A, Pages 1248-1263

Wanga H., Baia P., Zhoua H., Coehoornb R., Lic N., Liaoe H., Zhoua G. (2019), "An integrated heat pipe coupling the vapor chamber and two cylindrical heat pipes with high anti-gravity thermal performance", *Applied Thermal Engineering*, Volume 159, 113816

Weibel J. A., Garimella S. V. (2012), "Visualization of vapor formation regimes during capillary-fed boiling in sintered-powder heat pipe wicks", *International Journal of Heat and Mass Transfer,* Volume 55, Issues 13–14, Pages 3498-3510

Yarin A. L., Pourdeyhimi B., and Ramakrishna S. (2014), *"Nanofibers and applications"*, Cambridge University Press, Cambridge, 2014

Zohuri B. (2011), *“Heat pipe design and technology”*, Springer International Publishing Switzerland, 2016

CIRRICULUM VITAE

PRATISH SHINDE

Department of Mechanical and Industrial Engineering, University of Illinois at Chicago (UIC)

842 W. Taylor Street, Chicago, IL 60607-7022

EDUCATION

University of Illinois at Chicago, Chicago, IL, USA *Aug 2018 – May 2020*

- Candidate of Master of Science in Mechanical Engineering

Savitribai Phule Pune University *Aug 2015 – June 2018*

- B.E., Mechanical Engineering

Sandip Foundation's Sandip Polytechnic *Aug 2013 – June 2015*

- Diploma in Mechanical Engineering

TEACHING

Graduate Teaching Assistant – University of Illinois at Chicago

Fluid Mechanics, ME211 *Spring 2020*

- Instructed the laboratory section of the course

Numerical Methods in Mechanical Engineering, ME428 *Summer 2019*

- Grader and course teaching assistant

Fluid Mechanics, ME211 *Spring 2020*

- Grader and course teaching assistant